

SYNTHESIS AND REDUCTION OF COPPER-COAGULATED, GRAPHENE
OXIDE, FREE-STANDING THIN FILMS

by

Goutham Gunanjipalli

Copyright © Goutham Gunanjipalli 2018

A Thesis Submitted to the Faculty of the

COLLEGE OF OPTICAL SCIENCES

In Partial Fulfillment of the Requirements

For the Degree of

MASTER OF SCIENCE

In the Graduate College

THE UNIVERSITY OF ARIZONA

2018

STATEMENT BY AUTHOR

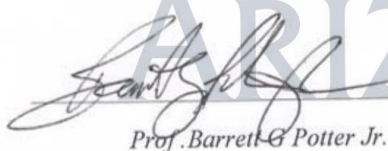
The thesis title *Synthesis and reduction of copper-coagulated, graphene oxide, free-standing thin films* prepared by Goutham Gunanjipalli has been submitted in partial fulfillment of requirements for a master's degree at the University of Arizona and is deposited in the University Library to be made available to borrowers under rules of the Library.

Brief quotations from this thesis are allowable without special permission, provided that an accurate acknowledgement of the source is made. Requests for permission for extended quotation from or reproduction of this manuscript in whole or in part may be granted by the head of the major department or the Dean of the Graduate College when in his or her judgment the proposed use of the material is in the interests of scholarship. In all other instances, however, permission must be obtained from the author.

SIGNED: Goutham Gunanjipalli

APPROVAL BY THESIS DIRECTOR

This thesis has been approved on the date shown below:


Prof. Barrett G. Potter Jr.

Professor, Dept. of Material Sciences and Engineering
College of Optical Sciences

Defense date

5/8/2018

ACKNOWLEDGEMENT

I would like to thank my advisers Prof. Barrett G. Potter Jr., and Prof. Krishna Muralidharan for their continuous support and mentoring throughout my research work. I would also like to extend my gratitude to Prof. Srini Raghavan for his advice with my research. I am grateful to Prof. Douglas Loy for allowing me to use his lab equipment.

I would like to thank to Dr. Sahila Perananthan who always helped me with my research and guided me whenever required. I would also like to extend my gratitude to the other group members Pratish Rao, Anna Hayes, Susana Castillo, Kathleen Fitzgerald Van Atta and Mason for their support.

Another thank you goes to my friends and family, who have always supported me unconditionally in all aspects of my life.

List of Contents

List of Figures	7
List of Tables	13
List of Abbreviations	14
Abstract	15
Chapter 1 : Background	17
1.1 Introduction.....	17
1.2 Synthesis of GO	18
1.3 Mechanism of Oxidation	21
1.4 GO structure models	24
1.5 Coagulation of divalent metal ions in GO	26
1.6 Reduction of GO	29
1.6.1 Thermal Reduction	29
1.6.2 Chemical Reduction.....	32
1.6.3 Microwave and Photo-reduction	35
1.7. Applications of GO and reduced GO.....	37
1.7.1 GO/rGO membranes and paper-like materials	37

1.7.2 GO/rGO in electronic devices	38
1.7.3 GO/rGO as energy storage devices	38
1.8 Present challenges and future research in GO/rGO	39
1.9 Thesis Overview	40
Chapter 2 : GO/rGO Characterization Techniques.....	41
2.1 X-ray Photoelectron Spectroscopy	41
2.2 Fourier Transform Infrared Spectroscopy (FTIR).....	43
2.3 Scanning Electron Microscopy (SEM).....	46
2.4 Four-Point Probe.....	49
Chapter 3 : Materials and Methods.....	51
3.1 Introduction.....	51
3.2 Graphene Oxide Synthesis: Modified Hummer's Method.....	51
3.3 Coagulation of GO suspension with Copper (Cu^{2+}) ions	54
3.4 Fabrication of GO and GO- Cu^{2+} free standing thin films via doctor blading	56
3.5 Low temperature thermal annealing of GO and GO + Cu^{2+} thin films	60
3.6 Laser reduction of GO + Cu^{2+} free-standing thin films.....	62
Chapter 4 : Results & Discussion	65

4.1 Chemical analysis using XPS	65
4.2 Morphology and elemental analysis using SEM & EDS	72
4.3 FT-IR Spectrum Analysis	79
4.3.1 FT-IR spectrum of GO and GO + Cu ²⁺ thin films.....	79
4.3.2 FT-IR spectrum of thermally reduced rGO + Cu ²⁺ thin films with different concentrations of Cu ²⁺	81
4.3.3 FT-IR spectrum of laser reduced GO + Cu ²⁺ (50 mM) irradiated with constant power and varying time.....	84
4.3.4 FT-IR spectra of laser reduced GO + Cu ²⁺ (50 mM) irradiated with constant time and varying power.....	85
4.4 Resistivity measurement using four-point probe.....	87
4.5 Conclusion & Future Scope.....	89
References	92

List of Figures

Figure 1.1 A schematic showing a comparison between Hummer's, modified Hummer's method and Tour's method (improved) [11].	20
Figure 1.2 Conversion of bulk graphite into GO in modified Hummers' method [15]	23
Figure 1.3 Proposed models for chemical structure of GO [19].	24
Figure 1.4 the structure model of GO with oxygen groups adhered on the surface. The as prepared GO and oxidative debris can be separated by base washing [18].	26
Figure 1.5 (a) GO (left) and GO + Cu ²⁺ (right) dispersions and thin film of GO + Cu ²⁺ formed by vacuum filtration of solution, (b) Schematic model for reaction between GO and Cu ²⁺ , (c) Images of GO and GO + Cu ²⁺ before and after flash reduction, (d) proposed model for the enhanced mechanical properties of GO paper observed after metal modification.	28
Figure 2.1 Schematic diagram of XPS process [76].	42
Figure 2.2 The C1s spectrum of (a) GO (b) rGO [38].	43
Figure 2.3 Interferometry setup for FTIR spectroscopy [77]	44
Figure 2.4 FTIR spectra of GO and rGO [78].	45
Figure 2.5 Electron beam interaction volume [79].	47
Figure 2.6 Schematic of Scanning Electron Microscope [93].	48

Figure 2.7 SEM images of (a) GO film, (b) rGO film [80].	49
Figure 2.8 Schematic of four point probe configuration [81]	50
Figure 3.1 Schematic flow-chart of all the steps involved in modified Hummer's method for synthesis of GO.	52
Figure 3.2 (a) Mixture of graphite powder, KMnO_4 , and H_2SO_4 , (b) Reaction mixture upon addition of H_2O_2 and DI water which makes the mixture brown, (c) Reaction mixture left undisturbed overnight, GO solution (d) after centrifugation, and (e) after sonication steps.	53
Figure 3.3 The interaction between GO and metal ion cross-linkers [31].	55
Figure 3.4 (a) Schematic model of the interaction of Cu^{2+} ions with GO and its functional groups, (b) $\text{CuSO}_4 \cdot 5 \text{H}_2\text{O}$ in water, (c) pH corrected GO with 6mg/ml concentration, (d) Addition of $\text{CuSO}_4 \cdot 5 \text{H}_2\text{O}$ to GO solution under continuous stirring (~250 rpm), and (e) GO coagulated with Cu^{2+} ions with different concentration of Cu^{2+} (10, 20, and 50 mM from left).	56
Figure 3.5 (a) Principle of doctor blading using a frame with reservoir of coating material which is moving relatively to the surface, (b) Thickness control of the thin layer by the gap between the frame (blade) and the substrate [86].	58
Figure 3.6 (a) Different of concentrations (10, 20, and 50 mM) of Cu^{2+} in GO dispersion (from left side), (b) Side view of a doctor blade coating process on a glass substrate, (c) Top view of a doctor blade coating process, and (d) Free standing film	

(GO + Cu²⁺ film of thickness 50 μm) obtained from doctor blade coating process (after peeling the film from the substrate).59

Figure 3.7 Schematic of the reduction of graphene oxide into reduced graphene oxide by thermal treatment [89].61

Figure 3.8 (a) Vacuum oven with temperature and vacuum control (Courtesy: Prof. D.A. Loy's lab) (b) GO + Cu²⁺ 50 μm thin film sandwiched between two glass slide before the thermal reduction (c) GO + Cu²⁺ free standing film after and before the thermal reduction at 170 °C for 90 minutes.62

Figure 4.1 XPS survey spectra of GO + Cu²⁺ before (a) and after (b) thermal reduction in vacuum at 170 °C for about 90 minutes. GO-Cu²⁺ before reduction has a C/O ratio of ~ 0.75 . After the low temperature thermal reduction, the oxygen content decreased and the C/O ratio increased to ~ 1.267

Figure 4.2 XPS C1s spectra of GO + Cu²⁺ before (a) and after (b) low temperature thermal reduction in vacuum at 170 °C for 90 minutes. Before reduction, the C1s peak analysis of the unreduced GO+Cu²⁺ films reveal the presence of oxygen containing functionalities in the form of epoxy, hydroxyl, and carbonyl groups. After thermal reduction, the peaks associated with the oxygen containing functionalities are diminished, and the predominance of the sp² hybridized carbon peak (blue curve peak position at ~ 284.798 eV) confirms graphene formation.68

Figure 4.3 XPS Cu2p spectra of GO + Cu²⁺ before (a) and after (b) low temperature thermal reduction in vacuum at 170 °C for 90 minutes. Before reduction, the Cu2p peak analysis of the unreduced GO + Cu²⁺ film reveals the presence of copper ions (~934.4 eV) and their predominant oxidation state is 2+. After reduction, the peaks corresponding to Cu2p remained unchanged and the predominant oxidation state of copper was 2+.69

Figure 4.4 (a) SEM image of GO film (50 μm) (b) SEM image of GO coagulated with 50 mM Cu²⁺ (50 μm thick).74

Figure 4.5 Typical SEM image of thermally reduced GO + Cu²⁺ (50 μm) film at 170 °C for 90 minutes under vacuum (b) SEM image of a laser reduced GO + Cu²⁺ (50 μm) film with a fluence of 75 mJ/cm².74

Figure 4.6 (a) SEM image of reduced GO film (50 μm) via low temperature thermal reduction (b) Distribution map of carbon over the scanned area of rGO film. (c) Distribution map of oxygen over the scanned area of rGO film (d) EDS spectrum of rGO film (50 μm) reduced via thermal reduction.....75

Figure 4.7 (a) SEM image of reduced GO + Cu²⁺ film (50 μm) with 10 mM CuSO₄ via low temperature thermal reduction (b) Distribution map of carbon over the scanned area of reduced GO + Cu²⁺ film. (c) Distribution map of oxygen over the scanned area of reduced GO + Cu²⁺ film (d) Distribution map of copper over the scanned area of reduced GO + Cu²⁺ film (e) EDS spectrum of reduced GO film (50

μm) reduced via thermal reduction (f) Elemental composition of reduced GO + Cu^{2+} (10 mM) film.....76

Figure 4.8 (a) SEM image of reduced GO + Cu^{2+} film (50 μm) with 20 mM CuSO_4 via low temperature thermal reduction (b) Distribution map of carbon over the scanned area of rGO + Cu^{2+} (20 mM) film. (c) Distribution map of oxygen over the scanned area of rGO + Cu^{2+} (20 mM) film (d) Distribution map of copper over the scanned area of rGO + Cu^{2+} (20 mM) film (e) EDS spectrum of rGO film (50 μm) reduced via thermal reduction (f) Elemental composition of rGO + Cu^{2+} (20 mM) film.77

Figure 4.9 (a) SEM image of reduced GO + Cu^{2+} film (50 μm) with 50 mM CuSO_4 via low temperature thermal reduction (b) Distribution map of carbon over the scanned area of rGO + Cu^{2+} (50 mM) film. (c) Distribution map of oxygen over the scanned area of rGO + Cu^{2+} (50 mM) film (d) Distribution map of copper over the scanned area of rGO + Cu^{2+} (50 mM) film (e) EDS spectrum of rGO film (50 μm) reduced via thermal reduction (f) Elemental composition of rGO + Cu^{2+} (50 mM) film.78

Figure 4.10 Representative FT-IR spectra of GO (50 μm thin film) and GO + Cu^{2+} (with 50 mM Cu^{2+} concentration and 50 μm thin film thickness).....80

Figure 4.11 Representative FT-IR spectra of GO and GO + Cu^{2+} coagulated with different Cu^{2+} concentrations; 10, and 50 mM.81

Figure 4.12 Representative FT-IR spectra of GO + Cu ²⁺ (50 mM Cu ²⁺) and thermally reduced rGO + Cu ²⁺ (50 mM Cu ²⁺).	82
Figure 4.13. Representative FT-IR spectrum of thermally reduced rGO and rGO + Cu ²⁺ thin films with different concentrations of Cu ²⁺ ; 10, 20, and 50 mM.	83
Figure 4.14 Representative FT-IR spectra of laser reduced GO + Cu ²⁺ (with 50 mM Cu ²⁺) at constant power of 0.5 mW/cm ² and varying time from 0, 10, 20, 40, 80 and 160 minutes.	85
Figure 4.15. FT-IR spectra of laser reduced GO + Cu ²⁺ (50 mM Cu ²⁺) thin films for a constant time of 5 minutes and varying power from 0.08, 0.25, 0.42, and 0.5 mW/cm ²	86
Figure 4.16 Picture of Bridgetec four-point probe.	87
Figure 4.17. Plot showing resistivity of thermally reduced rGO + Cu ²⁺ with increase in Cu ²⁺ concentration (10, 20, and 50 mM)(k Ω /□) as a function of concentration of Cu ²⁺ (mM).	89

List of Tables

Table 1-1 Comparison of methods for GO synthesis	21
Table 1-2 Summary of thermal reduction methods for GO.....	31
Table 1-3 Summary of chemical reduction methods for GO	34
Table 3-1 Thermal reduction conditions for GO and GO + Cu ²⁺ free standing thin films.....	61

List of Abbreviations

CCG	Chemically converted graphene
Cu^{2+}	Copper ions
EDS	Electron dispersive spectroscopy
ESCA	Electron spectroscopy for chemical analysis
FPP	Four-point probe
FTIR	Fourier transform infrared
GO	Graphene Oxide
$\text{GO} + \text{Cu}^{2+}$	Graphene oxide coagulated with copper ions
MAS- NMR	Magic angle spinning nuclear magnetic resonance
PET	Polyethylene terephthalate
rGO	Reduced Graphene Oxide
$\text{rGO} + \text{Cu}^{2+}$	Reduced graphene oxide coagulated with copper ions
SEM	Scanning electron microscopy
XPS	X- ray photoelectron spectroscopy

Abstract

As a two-dimensional material, graphene has attracted great interest among the research groups and the industry due to its exceptional electrical, optical and mechanical properties. Currently, the primary methods for mass production of graphene are focused on the solution-processable chemical redox reaction. The oxidation of graphite introduces a large amount of oxygen functional groups attached onto its basal plane or edges, which makes graphene oxide (GO) sheets hydrophilic to form stable dispersions. However, the starting material graphite gradually becomes an insulator during the oxidation process as a part of planar sp^2 -hybridized geometry transformed to distorted sp^3 -hybridized geometry, which decreases the electrical conductivity. As a result, the reduction of GO is essential to recover graphene-like electrical conductivity for practical applications. In addition, the hydrophilic property of GO sheets allows coagulation of divalent metal ions in GO. These ions attach onto the GO basal plane and interact with functional groups resulting in GO/metal ion hybrid thin films with excellent electrical conductivity after reduction.

In this work, the effect of coagulation of GO using copper ions (Cu^{2+}) on optical and electrical properties of graphene oxide and reduced graphene oxide is studied. Two different reduction schemes were examined: direct, low-temperature annealing in vacuum and laser reduction of GO and GO-Copper films. This study includes the

preparation of GO and GO-Cu stable dispersions, the fabrication of free standing thin films using a doctor blade process, the GO reduction, and the structural and electrical conductivity characterization of the resulting materials. Structural studies involved Fourier transform infrared spectroscopy (FTIR) and scanning electron microscopy/ Electron dispersive spectroscopy (SEM/EDS). A four-point probe measurement was used to examine film electrical resistivity.

Chapter 1 : Background

1.1 Introduction

A monolayer of carbon atoms with a two-dimensional honeycomb structure and sp^2 hybridized bonding is referred to as ‘graphene’ [1]. The first isolation of freestanding graphene was reported in 2004 [2]. Graphene exhibits a zero eV bandgap and has a thickness of about 0.34 nm [3]. Over the past decade, graphene has enjoyed significant attention from researchers due to its exceptional physical properties, including: high electrical conductivity ($\sim 10^6$ s/cm), good optical transmittance ($\sim 97.7\%$), high Young’s modulus (~ 1.0 TPa), high thermal conductivity (~ 5000 Wm $^{-1}$ K $^{-1}$) and high intrinsic mobility ($\sim 2 \times 10^5$ cm 2 s $^{-1}$) [4]. These properties of graphene make it attractive for electronic and optoelectronic applications.

Synthesis of high-quality graphene with high yield using an economical process is of key importance to enhance the study of this material and its potential for use in applications [5]. Graphene sheets can be prepared using two primary approaches: bottom-up and top-down processing. In the bottom-up approach, graphene sheets are produced by deposition from the gas phase using carbon-containing molecules such as methane or ethanol. On the other hand, the top-down approach involves exfoliating individual graphene sheets from graphite [6]. For high-yield and low-cost manufacturing, the top-down approach (involving chemical oxidation,

exfoliation and reduction) proves to be most promising route. In this process, bulk graphite is first converted into graphite oxide using chemical oxidizing agents. The as-synthesized graphite oxide is further exfoliated to graphene oxide (GO). Lastly, GO can be converted into graphene-like material, referred as reduced graphene oxide (rGO), using different reduction methods and reducing agents. The synthesis and application of graphene produced by a wet-chemical top-down method has been a topic of significant interest in the field of graphene.

1.2 Synthesis of GO

The first synthesis of GO was demonstrated by B.C Brodie in the nineteenth century [7]. In this experimental approach, Brodie mixed known amounts of graphite with potassium chlorate and reacted this mixture in fuming nitric acid. After rinsing to remove the salt products from the reacted materials, the resulting material was re-oxidized under the same conditions three more times to obtain a light yellow colored crystal. The composition ratio of the final product C: H: O was found to be 61.04: 1.85: 37.11, indicating a formula of $C_{11}H_4O_5$. Brodie named this material as “Graphic acid” [7].

Another chemist named, L.Staudenmaier improved Brodie’s process by adding concentrated sulfuric acid and multiple aliquots of potassium chlorate to the reacting mixture [8]. This resulted in a final product with similar elemental composition ratio

to Brodie's process but in a single step oxidation process, though potassium chlorate was added over a period of 7 days [8].

Hummer's and Offeman demonstrated a fast and different oxidation strategy by reacting graphite with a mixture of potassium permanganate (KMnO_4), concentrated sulfuric acid, and sodium nitrate [9]. This method required less time and avoided the use of highly corrosive fuming nitric acid. Although Hummer's method contains a large quantity of incompletely oxidized graphite it has been adopted by other researchers for the oxidation of graphite [9]. Later on, a modified Hummer's method was demonstrated that treated the starting material graphite with a mixture of concentrated H_2SO_4 , $\text{K}_2\text{S}_2\text{O}_8$, and P_2O_5 by [10].

Both Hummer's and modified Hummer's method resulted in toxic by-products such as NO_2 and N_2O_4 due to the use of sodium nitrate [11]. In order make it a more eco-friendly process; Tour's research group reported a new method. This approach made use of phosphoric acid rather than sodium nitrate and increased the amount of potassium permanganate [11]. Tour's method claims to produce higher yield than Hummer's or modified Hummer's method. These three methods are summarized in Figure 1.1 below.

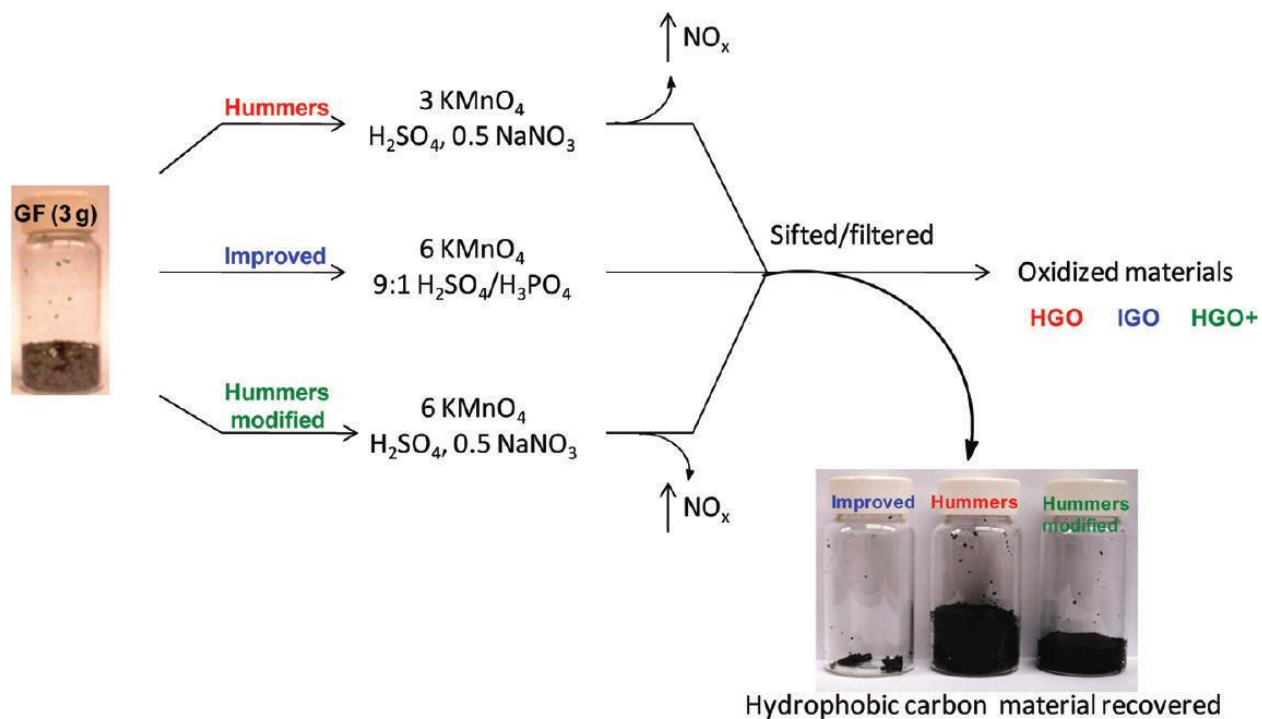


Figure 1.1 A schematic showing a comparison between Hummer's, modified Hummer's method and Tour's method (improved) [11].

Peng et al. [12] developed a new method for GO formation that used K_2FeO_4 instead of KMnO_4 . As this oxidant is more environment friendly and produced high yield, this method can be adopted for mass production [12]. The synthesis of GO has evolved over many years of research to improve the synthesis of graphene to making it more efficient and environmentally friendly. Table 1-1 lists a range of GO synthesis methods and their associated characteristics.

Table 1-1 Comparison of methods for GO synthesis

Method	Reactants	Reaction Time	Reaction temperature(° C)	C/O	By-products
Brodie(1859) [7]	KClO ₃ , HNO ₃	3-4 days	60	2.16	ClO ₂
Staudenmaier(1898) [8]	KClO ₃ , HNO ₃ , H ₂ SO ₄	1-10 days	RT	-	ClO ₂ , NO _x
Hummers(1958) [13]	H ₂ SO ₄ , KMnO ₄ , NaNO ₃	2 h	35	2.25	NO _x
Modified Hummers(1999) [10]	H ₂ SO ₄ , K ₂ S ₂ O ₄ , P ₂ O ₅ , KMnO ₄ , NaNO ₃	6h 2h	80 35	2.3	NO _x
Tour(2010) [11]	H ₂ SO ₄ , KMnO ₄ , H ₃ PO ₄	12h	50	-	-
Peng(2015) [12]	H ₂ SO ₄ , K ₂ FeO ₄	1h	RT	2.2	NO

1.3 Mechanism of Oxidation

The formation of graphene oxide typically involves the intercalation of molecular species into graphite to create isolated GO sheets. In one of the proposed

mechanism, acid ions and an oxidizing agent intercalate into the interlayer spaces within the graphite and react with the carbon atoms to form oxide functional groups on the layer surface. Van der Waals forces between the carbon layers is thus weakened, allowing the graphene oxide sheets to be exfoliated by dispersion in water or via sonication [14].

Alternatively, Dimiev and Tour [15] suggested a mechanism for the formation of graphene oxide based on the modified Hummers' method in which the intercalation, oxidation reaction, and exfoliation steps are separated. In this proposal, graphite is converted into GO in three steps, as shown in Figure 1.2. The first step begins with mixing graphite with an acidic oxidizing medium. This process forms a sulfuric acid-graphite intercalation compound (H_2SO_4 - GIC). The second step involves converting the GIC into graphite oxide. In the second step, an oxidizing agent replaces the intercalant molecules by diffusion into the interlayer galleries resulting in the reaction with carbon atoms. The third step consists of the conversion of graphite oxide to GO. When the graphite is completely oxidized, the GO will exfoliate to monolayer GO upon the introduction of water [15]. Here, the enthalpy of hydration of the charged GO layers by water overcomes the electrostatic attraction between adjacent layers in the graphite oxide [16].

This approach allowed a more comprehensive understanding of GO formation. Even though the identity of the oxidizing agent species reacting with

graphite interlayers is still unclear, knowing the diffusion mechanism of the oxidizing agent can lead to better control over the reaction process. The reaction time for full oxidation of graphite can be decreased by utilizing a high mesh graphite source, i.e. having a smaller particle size graphite powder.

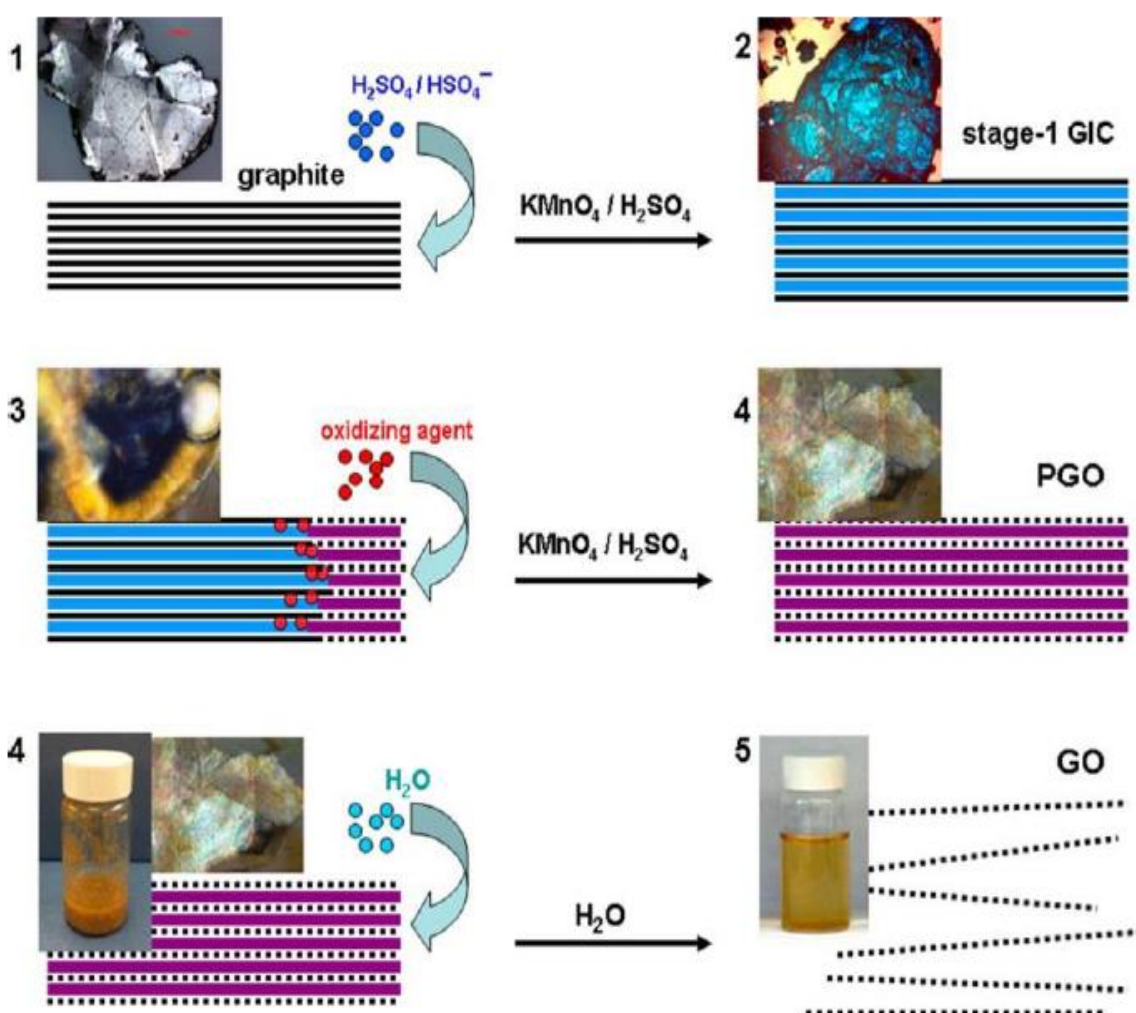


Figure 1.2 Conversion of bulk graphite into GO in modified Hummers' method [15]

1.4 GO structure models

Despite the long history of GO synthesis development, the precise chemical structure of GO is still under debate. The limited applicability of analytical techniques to the effective unambiguous characterization of such materials and the complex structure of GO [17] is a primary contributor. Studies have found that the structure of GO is dependent upon both the oxidation process and the characteristics of the starting material used, i.e. graphite [18]. Thus, describing the chemical structure of GO is challenging. Several structural models of GO have been proposed over the years, including those of Hofmann Ruess, Scholz-Boehm, Nakajima-Matsuo, Lerf-klinowski, and Dekany [19] models as shown in the Figure 1.3.

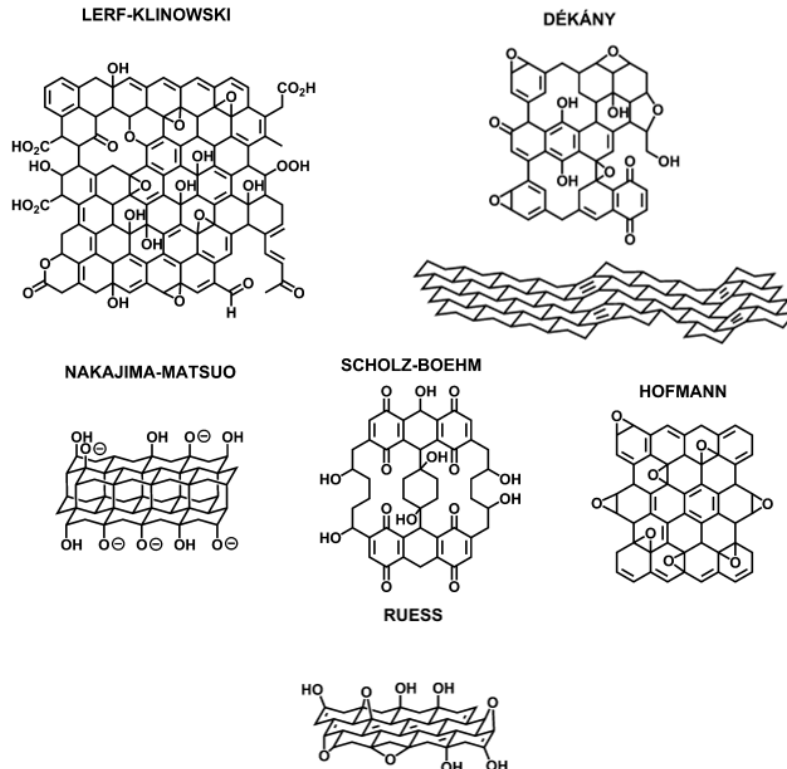


Figure 1.3 Proposed models for chemical structure of GO [19].

The first chemical structural model of GO was proposed by Hofmann and Holst, and consisted of repeating units of epoxy groups on the basal plane of the graphene with a molecular formula C_2O [9]. Ruess further modified this model, with incorporation of hydroxyl groups into the carbon basal plane based on the discovery of H_2 atoms in GO [20]. Ruess's model contained sp^3 hybridized basal planes unlike the Hofmann's which had sp^2 hybridized bonds.

Two decades later, Scholz and Boehm proposed a GO structure contains hydroxyl and ketone groups with a corrugated backbone of carbon atoms [21]. Meanwhile, Nakajima and Matsuo suggested a new model for GO chemical structure, which contained two carbon layers linked by sp^3 carbon-carbon atoms, hydroxyl and carbonyl groups [22]. Lerf and Klinowski put forward a model for GO by analyzing the GO material using a magic-angle spinning nuclear magnetic resonance (MAS-NMR) technique. This model contained randomly distributed unoxidized aromatic sections with benzene rings (graphene-like) and oxidized regions with sp^3 hybridized carbon rings [23]. In addition, functional groups, such as hydroxyl and epoxide were proposed to decorate the oxidized regions on the basal plane, whereas carboxylic acids were distributed around the edges of the sheet. This model serves as the current reference and it is widely accepted, with confirmation from experimental observations using high-resolution transmission electron microscopy [24].

More recently, Dekany et al. proposed another model for the structure of GO based on comprehensive characterization and analysis. In this case, GO was described in terms of two structural regions: 1. corrugated hexagonal ribbons and 2. Trans-linked cyclohexane chairs [19]. Wilson's group [25] published a new structural model of GO, which showed that GO synthesized using modified Hummer's method is composed of functionalized graphene-like sheets with strongly adhered oxidative debris. This debris layer acts as a surfactant to stabilize GO in water [25]. This oxidative debris can be removed by base washing with aqueous sodium hydroxide (NaOH) or aqueous ammonia to obtain a black aggregate that is more conductive than GO [26].

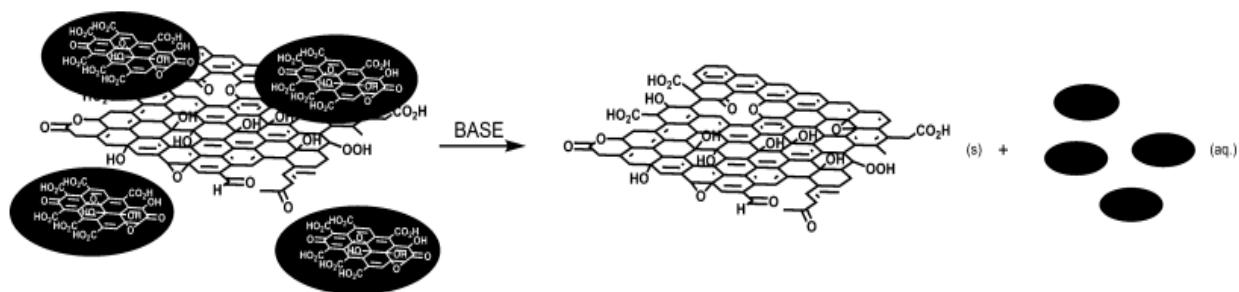


Figure 1.4 the structure model of GO with oxygen groups adhered on the surface. The as prepared GO and oxidative debris can be separated by base washing [18].

1.5 Coagulation of divalent metal ions in GO

As described above, graphene oxide can readily undergo exfoliation in water, yielding colloidal suspensions consisting of entirely individual graphene oxide sheets [27]. Graphene oxide has been considered hydrophilic due to its ready

dispersion in water and interfacial properties. This behavior can be tuned at the molecular level by functionalizing with radicals to introduce new properties [28] [29]. Positively charged groups can be introduced to bind with these negatively charged GO sheets.

GO has oxygen-containing functional groups present at the edges and on the basal planes. These groups offer the potential for modification and molecular level control of GO properties, enabling the fabrication of functional materials. In addition, the ionization of basal carboxyl groups is pH dependent [30] and can be used to bind divalent metal ions to GO sheets. Significant enhancement in mechanical stiffness (10-200%) and fracture strength (~50%) in graphene oxide paper was reported upon the addition of small amounts (<1 wt %) of Mg^{2+} and Ca^{2+} [31]. Different metal ions such as Fe^{2+} , silver, and gold nanoparticles can be added to GO dispersions to order to increase the magnetic properties [32] [33], to make substrates for surface enhanced Raman spectroscopy [34], and to be used in the field of sensing [35].

It has been reported that metallic ions binding to GO can increase its electrical conductivity. In this context, a hybrid graphene oxide material with Cu^{2+} ions bonded with the negatively charged functional groups on GO has been investigated and it was found that the electrical resistivity was dramatically decreased upon flash reduction [36].

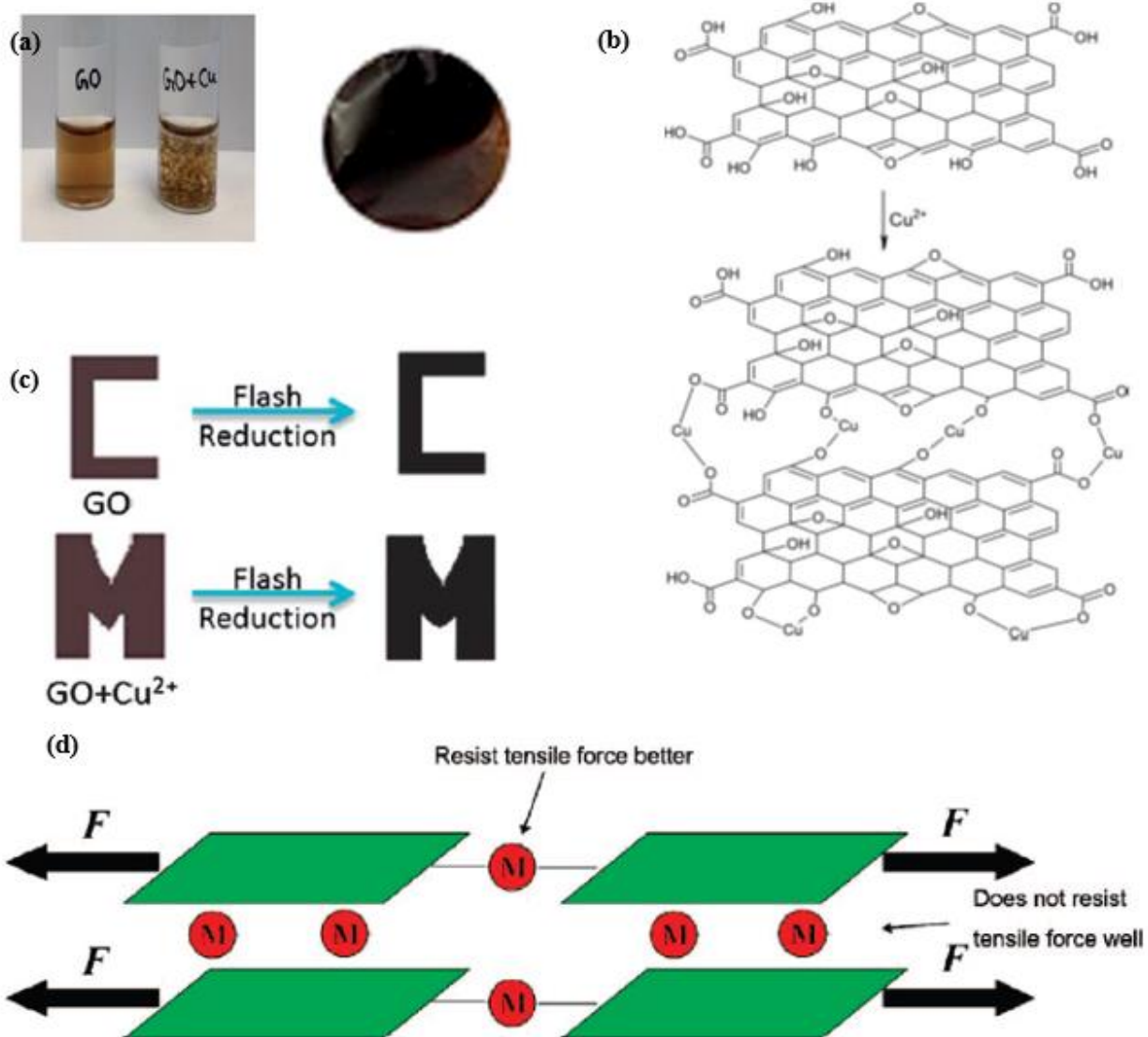


Figure 1.5 (a) GO (left) and GO + Cu²⁺ (right) dispersions and thin film of GO + Cu²⁺ formed by vacuum filtration of solution, (b) Schematic model for reaction between GO and Cu²⁺, (c) Images of GO and GO + Cu²⁺ before and after flash reduction, (d) proposed model for the enhanced mechanical properties of GO paper observed after metal modification.

1.6 Reduction of GO

Graphene is an electrically conducting material with conductivity values comparable to copper. Unlike graphene, GO is an electrically insulating material due to the presence of functional groups on the basal plane. The electrical conductivity is decreased significantly, as the oxidation process distorts the sp^2 carbon atoms of the network and converts them to a sp^3 hybridization, disrupting the π - π conjugation. [37]. “Reduction” involves the removal of excess oxide functional groups present in GO to recover the electrical conductivity behavior of the original graphene. Many strategies have been employed to reduce GO over the years. The resulting material is often referred to as reduced graphene oxide (rGO) and is also called chemically modified graphene oxide. We will limit our interest to thermal, chemical and photo-reduction techniques.

1.6.1 Thermal Reduction

Under appropriate conditions, thermal reduction has been found to be an efficient method to rapidly reduce GO. It has been demonstrated that graphite oxide powder can be exfoliated and converted to reduced graphene by rapid heating ($> 2000\text{ }^\circ\text{C/min}$), which leads to the decomposition of function groups into CO or CO_2 gases [38]. Reduced graphene oxide prepared by a thermal annealing process has a small flake size about $10\text{ }\mu\text{m}$ in diameter and shows a wrinkled structural surface

morphology [39]. This effect results from the decomposition of carbon atoms from the basal plane along with the functional groups into the gas or vacuum, which in turn produces topological defects throughout the carbon plane and a breakdown of the sheet structure [40]. The reduced GO prepared from thermal reduction has electrical conductivities of 1000-2300 Sm^{-1} [17]. While this number is several orders of magnitude higher than that of GO, it is still much lower than that of graphene. This is related to the degree of reduction and the extent of restoration of the π - π electronic structure in the basal plane that is achieved in the process [41].

An alternative method to produce reduced graphene oxide sheets with higher conductivity and lower defect densities is to disperse the GO sheets in a solvent first, then to deposit this GO dispersion as thin films on a substrate [42] or as a free-standing film [43]. The resulting material is then subjected to suitable thermal reduction conditions. Wang et al. reported the development of thermally reduced GO films at different reduction temperatures [42]. In this study, the conductivity of films at 550 °C was about 5000 Sm^{-1} , while those annealed at 1100 °C showed a conductivity of $5.5 \times 10^4 \text{ m}^{-1}$ an increase in conductivity of 5 times [42]. Further increase in the annealing temperature, e.g. to 2000 °C, results in complete decomposition of the oxygen-containing functional groups on the GO and a decrease in structural defect density due to the restoration of carbon framework [44].

Usually, a considerable mass loss of GO is observed upon heating at high temperatures ($>500\text{ }^{\circ}\text{C}$), attributed to the deoxygenation process. Therefore, to avoid the increase in defect population in the resulting reduced GO sheets, many research groups have explored various methods to reduce the reduction temperature required. These methods included treating the GO with organic solvents before thermal reduction to lower the thermal stability of the graphene oxide and its deoxygenation temperature or the use of vacuum or under controlled atmospheres (N_2 , Ar etc.) during thermal treatment [45]. An ultra-low temperature, solvothermal process has also been utilized to produce reduced graphene oxide (rGO)/ZnO nanocomposites. This study demonstrated a non-surfactant based, in-situ preparation of rGO/ZnO with the reduction of GO achieved at temperatures $<170\text{ }^{\circ}\text{C}$ [45]. Table 1-2 shows the summary of the thermal reduction methods for GO.

Table 1-2 Summary of thermal reduction methods for GO

Thermal Reduction Conditions	Time	Conductivity(Sm^{-1})	C/O ratio
Rapid heating ($>2000\text{ }^{\circ}\text{C}/\text{min}$) 1050 $^{\circ}\text{C}$ in Argon [38]	30s	1000 – 2300	10
550 $^{\circ}\text{C}$ in Argon or H_2 [42]	-	5×10^3	-
1100 $^{\circ}\text{C}$ in Argon or H_2 [42]	-	5.5×10^4	-
1500 $^{\circ}\text{C}$ in Argon [43]	1h	1.71×10^5	>1000
2700 $^{\circ}\text{C}$ in Argon [43]	1h	5.77×10^5	>1000

1.6.2 Chemical Reduction

Although, thermal reduction serves as viable method to obtain high quality reduced graphene oxide from GO, this process is not practical in all cases because of its high-energy cost and incompatibility with common substrates like plastic, PET (polyethylene terephthalate) etc. [46]. Removal of oxygen containing functional groups can also be achieved using chemical reductants at room temperature or with minimal heating. Most of the chemically reducing agents not only react and remove the oxygen containing functional groups but also can form new groups in their place, which may in turn functionalize the reduced graphene oxide. Thus, rGO produced via chemical reduction techniques is also referred as chemically converted graphene (CCG) [47].

Hydrazine (N_2H_4) is one of the most commonly used chemical reducing agents for synthesizing CCG. Reduction of GO using hydrazine was demonstrated by Ruoff and his co-workers [48]. In this work, they added hydrazine hydrate to a GO aqueous colloidal suspension and the conductivity of the resulting reduced graphene oxide (rGO) was about 2400 Sm^{-1} , which was 5 orders of magnitude higher than that of GO. Dan et al. [49] reported that the conductivity of CCG (reduced by hydrazine) is related to the weight ratio of hydrazine and GO. Optimization of this ratio produced a conductivity of 7200 Sm^{-1} at the room temperature [49]. However,

due to its high toxicity and potential hazards, hydrazine is not suitable for large-scale practical applications. Hydroiodic acid (HI) has also been used as a reducing agent to obtain highly conductive reduced GO. Pei and his research group achieved a CCG with conductivities of the order 10^4 Sm^{-1} with a C/O ratio of 12 by immersing the graphene oxide thin film in hydroiodic acid at 100°C [50]. A mixture of hydroiodic acid and acetic acid has also been employed as a suitable reducing agent at a temperature of 40°C [51]. Furthermore, due to the low vapor pressure of the HI, GO can be efficiently reduced in a gas-phase reaction environment (HI fumes) [51].

Ascorbic acid, well known as Vitamin C, is also used as a reducing agent for GO. It is considered an eco-friendly substitute for hydrazine. Zhang and his co-workers [52] first reported the efficient reduction of GO using ascorbic acid. In this work, they removed the oxygen-containing functional groups from GO by exposing it for 48 hours to ascorbic acid at room temperature. This resulted in a conductivity of 800 Sm^{-1} in the reduced GO [53]. By changing the quantity of ascorbic acid and increasing the reaction temperature to 95°C , the time of reduction can be shortened to 15 minutes while the conductivity of the reduced GO can reach 7700 Sm^{-1} . This is comparable to that of hydrazine reduction at similar conditions [52]. Reduction of GO has also been achieved with other eco-friendly reducing agents like alcohols and sugars [54] [55]. Nevertheless, the conductivity of CCG reduced by ascorbic acid is

always higher than that of other reducing agents. Table 1-3 shows the summary of all the chemical reduction methods for GO discussed.

Table 1-3 Summary of chemical reduction methods for GO

Chemical reducing Agents	Reduction temperature(°C)	Reduction Time	Conductivity(Sm⁻¹)	C/O ratio
Hydrazine hydrate [48]	100 °C	24h	2400	10.3
Hydrazine and ammonia solution [49]	95 °C	1h	~7200	~8
Ascorbic acid or vitamin C [52]	23 °C	24h	800	-
Hydrazine monohydrate & Ammonia solution [49]	95 °C	15min	9960	12.5
Vitamin C and ammonia solution [53]	95 °C	15min	7700	12.5
Aliphatic alcohols [54]	100 °C	5 days	1019	6.9
Benzyl alcohol [55]	100 °C	5 days	4600	30

Hydroiodic acid [50]	100 °C	1h	2.98×10^4	12
Hydroiodic acid and acetic acid [51]	40°C	40h	3.04×10^4	11.5

1.6.3 Microwave and Photo-reduction

Microwave and photo-reduction methods are rapid, chemical-free, and energy efficient when compared to the traditional chemical and thermal reduction processes [56]. Hassan et al. [90] synthesized stable rGO dispersions by heating the GO dispersions in a mixed solution of water and N, N-dimethylacetamide with microwave irradiation. The conductivity of rGO was found to be four orders of magnitude higher than that of GO. Zhu et al. also reported a rapid reduction of GO in a commercial microwave oven with 1 minute exposure to radiation [57].

Several research groups have demonstrated that GO can be reduced by photo-irradiation including, UV-induced photocatalytic reduction [58] [59], selective reduction by direct laser writing [60], photo-thermal reduction using a pulsed xenon flash [61] and laser converted graphene from GO [62]. The main advantage of such photo-reduction processes is that they do not rely on the use of chemicals or high

temperature and they can shorten the reduction time from several hours to a few minutes.

Lei Huang and his group [63] demonstrated the reduction of a GO dispersion using a KrF excimer laser that had a wavelength of 248 nm, a pulse width of 220 ns, maximum pulse energy of 700 mJ and a maximum repetition rate of 50 Hz. In a typical pulsed-laser reduction experiment, the laser energy was 200 mJ, the repetition rate was 5 Hz and the typical irradiation time was 5 minutes. Using these conditions, an rGO conductive sheet was obtained with a sheet resistance of $53.8 \text{ K}\Omega/\square$ [63].

Sokolov et al. [64] showed the direct observation of laser-induced, single-layer GO reduction examined via changes in optical absorption and emission. In this work, they have collected spatially resolved, time dependent absorption/emission images to follow the initial stages of single layer GO reduction, its transition to rGO, and its subsequent decomposition upon prolonged laser illumination. This correlated absorption/emission imaging provides great insight into the photo reduction mechanisms in GO and provided the GO/rGO absorption coefficients [64].

Many studies have attributed the light-induced reduction mechanism in GO to photolysis. In this mechanism, light is absorbed by a molecular resonance

associated with an oxygen-containing functional group. The absorbed energy then dissipates through radiative or non-radiative channels initiates a change in the chemical bonding associated with the functional group [65]. Specific GO functional group photolytic chemistries include OH, C-O-C, C=O, and COOH dissociation [66].

1.7. Applications of GO and reduced GO

In the last decade, GO and reduced or chemically converted GO have been widely used as a multifaceted material for various applications due to its exceptional properties. The dispersibility of GO in water and organic solvents and the availability of various reduction strategies makes possible the high-yield manufacture of graphene-based functional electronic devices through an eco-friendly and economically inexpensive solution-based processing.

1.7.1 GO/rGO membranes and paper-like materials

GO readily coagulates with multi-valent metal cations, forming hybrid materials, which enhances properties such as electrical conductivity, tensile strength, magnetic properties, thermal stability etc. of the GO [36] [31]. In the solid form, GO flakes tend to attach to one another (with or without the presence of metal cations), forming thin, and stable, paper-like structures that can be folded, wrinkled and

stretched. These freestanding GO films find use in applications like hydrogen storage, ion conductors, and nano-filtration membranes.

1.7.2 GO/rGO in electronic devices

GO/rGO has been used as a starting material to fabricate many electronic and optoelectronic devices. One such device is a graphene-based field effect transistor (FET) [67]. FETs that make use of rGO have also been used as chemical sensors [68] [69]. One of the major application areas of GO and rGO is in the production of transparent conductive films. Such thin films on a substrate can be used in flexible electronics, solar cells, and touch screen devices as a substitute of ITO (Indium-tin oxide) [70] [71].

1.7.3 GO/rGO as energy storage devices

As GO and rGO have a large surface area, these materials are considered for use as electrode materials in batteries, super-capacitors, fuel cells and solar cells [72]. Nanocomposites of GO/rGO can also be used for high-capacity energy storage in lithium ion batteries. In this regard, electrically insulating metal oxide Nanoparticles were adsorbed onto rGO to increase the efficiency of these materials in batteries [73]. Zhou and his co-workers fabricated the Li-ion battery using rGO wrapped Fe_3O_4 material and found that the energy storage capacity and cycle stability were increased compared to pure Fe_3O_4 [74].

1.8 Present challenges and future research in GO/rGO

The different applications of GO/rGO have been mentioned. Although the complete reduction of GO to reduced graphene is still difficult to achieve, partial reduction of GO can be readily attained. Nevertheless, GO sheets with a high concentration of lattice defects are difficult to fully reduce. The defects themselves are difficult to remove by post-treatment (thermal or chemical reduction techniques). Hence, a more controllable oxidation during the production of GO is needed to achieve highly reduced GO.

Further research on GO/rGO is needed, with focus on the reduction mechanism, controllable oxidation and reduction of GO, controllable functionalization of GO, and the coagulation of metal ions in GO. Enhanced control of functionalization and coagulation of GO can alter the properties of reduced graphene to satisfy the requirements of various applications [75]. Research on oxidation and reduction combined with increased understanding of the graphene structure may enable the realization of improved control over the attachment and elimination of functional groups and multivalent-cations at specific locations on the basal plane of carbon. This would, in turn, facilitate the application of graphene as semi-conductors used in electronic and optoelectronic devices.

1.9 Thesis Overview

In this work, the effect of pre-coagulation of GO using copper ions (Cu^{2+}) on optical and electrical properties of graphene oxide and reduced graphene oxide is studied. Two different reduction schemes were examined: direct, low-temperature annealing in vacuum and laser reduction of GO and GO-Copper films. This study involved the preparation of GO and GO-Cu stable dispersions, the fabrication of free standing thin films using a doctor blade process, the GO reduction, and the structural and electrical conductivity characterization of the resulting materials. Structural studies involved Fourier transform infrared spectroscopy (FTIR) and scanning electron microscopy/ Electron dispersive spectroscopy (SEM/EDS). A four-point probe measurement was used to examine film electrical resistivity.

Chapter 2 : GO/rGO Characterization Techniques

This chapter introduces some of the characterization and spectroscopic techniques used in the study of GO and GO + Cu²⁺ free standing thin films and their corresponding reduced form.

2.1 X-ray Photoelectron Spectroscopy

X-ray photoelectron spectroscopy (XPS), also known as electron spectroscopy for chemical analysis (ESCA), is a standard technique for analyzing the surface chemistry of a material. XPS can measure the elemental composition, chemical and electronic state of the elements within the material. In this technique, the sample is irradiated with beam of X-rays and the kinetic energies of the electrons ejected from the sample are measured. A spectrum is recorded by counting the ejected electrons over a range of kinetic energies. This spectrum enables the identification and quantification of the elements. The photoelectron process is shown in Figure 2.1, where an electron from K-shell is ejected from an atom as a 1s photoelectron after ionization by incident x-rays [76].

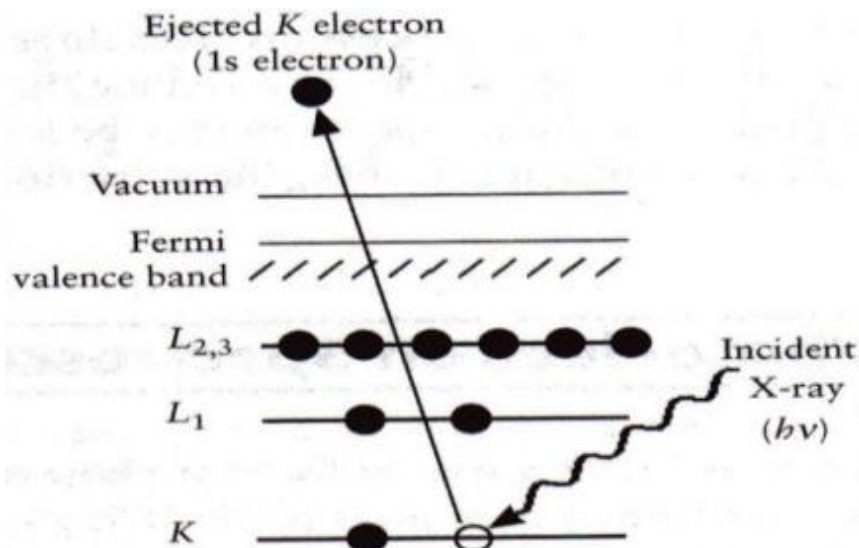


Figure 2.1 Schematic diagram of XPS process [76].

In fact, XPS is widely used in GO and rGO research to assess the efficiency of the reduction by calculating the carbon to oxygen atomic ratio and the binding energies of the functional groups [38]. Figure 2.2 shows the XPS spectrum for the C1s photoelectrons produced by a GO film and a reduced GO film (rGO). In figure 2.2(a), different functional groups exhibit different C1s binding energies in GO: C-O (~ 286.2 eV), C=O (~ 287.8 eV), C-C (~ 284.6 eV). After reduction, rGO (Figure 2.2(b)), shows a reduced intensity of C-O with an increase in C-C and therefore the atomic ratio is significantly reduced [38].

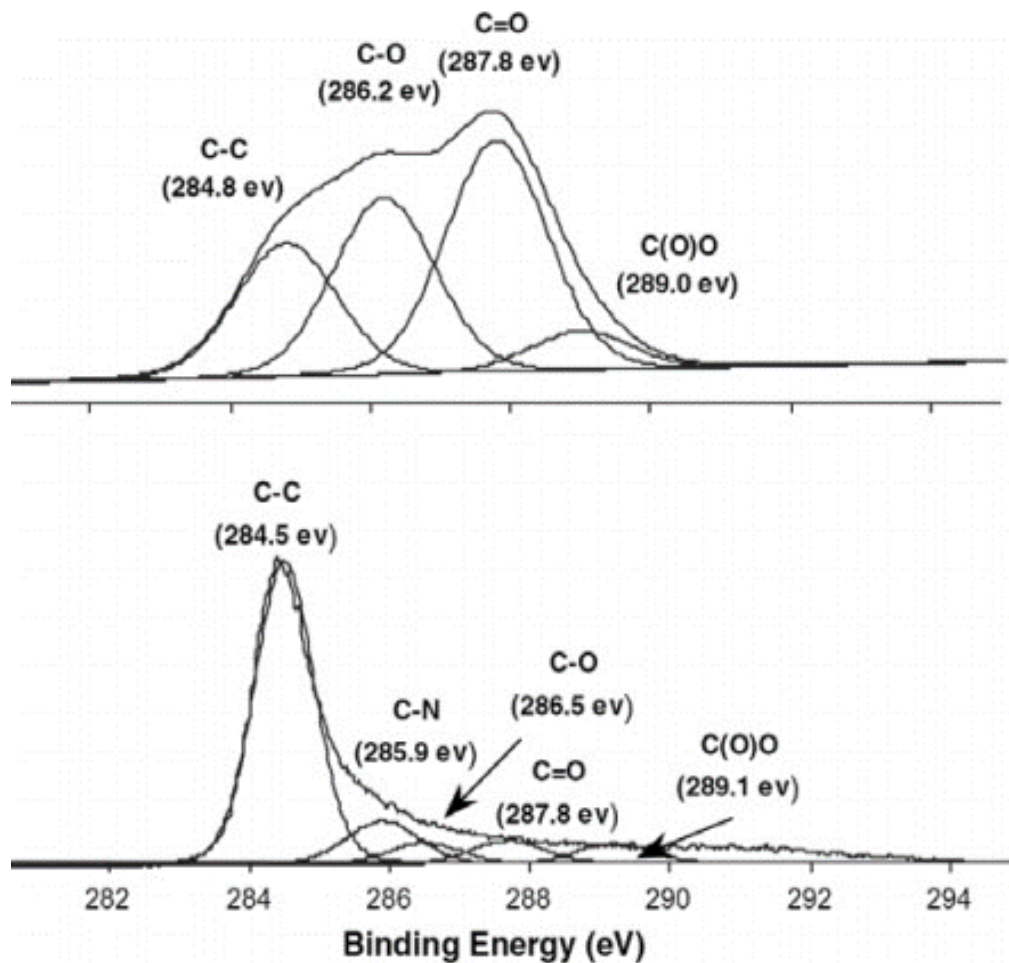


Figure 2.2 The C1s spectrum of (a) GO (b) rGO [38].

2.2 Fourier Transform Infrared Spectroscopy (FTIR)

In Fourier Transform Infrared (FTIR), spectroscopy infrared (IR) radiation is passes through a sample. Absorption by vibrational states in the material can cause some of the radiation to be absorbed by the sample. The resulting spectrum at the detector is thus dependent upon the molecular characteristic of the sample. An

analysis of the frequencies and intensities of absorption bands in the spectrum can therefore provide insight into the medium-range structure of the material.

FTIR spectroscopy can be classified into three categories: near infrared (NIR) (12800 to 4000 cm^{-1}), mid infrared (MIR) (4000 to 200 cm^{-1}), and far infrared (FIR) (50 to 1000 cm^{-1}). The absorption energies observed depends on the vibrational modes of the atomic structure (such as stretching, and bending), the mass of the atoms involved, and their bond strength. [4]. Figure 2.3 shows the schematic of an FTIR spectrometer. FTIR makes use of the principle of interferometry to produce a frequency-dependent assessment of material behavior [77].

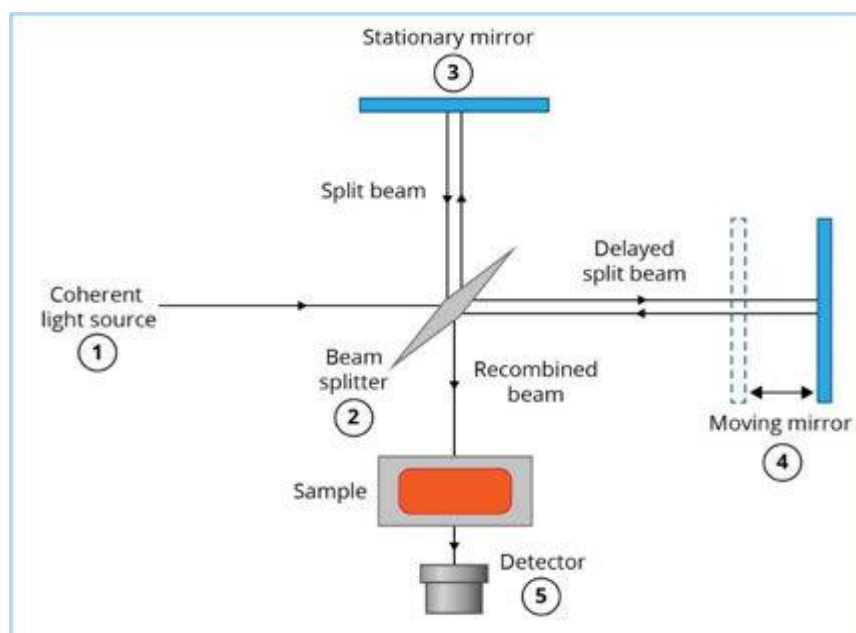


Figure 2.3 Interferometry setup for FTIR spectroscopy [77]

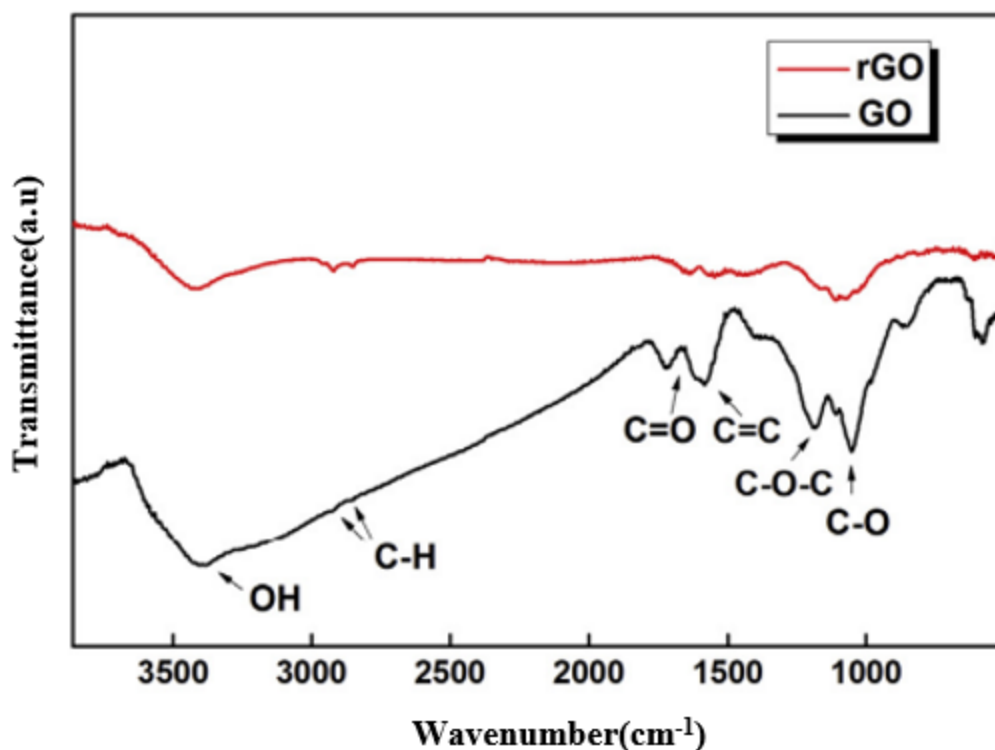


Figure 2.4 FTIR spectra of GO and rGO [78].

An FTIR spectrum is produced from a raw interferogram (intensity vs. scanning interferometer mirror position) via a Fourier transform. Figure 2.4 shows a typical transmittance spectrum of GO and rGO in the IR region recorded by FTIR spectrometer. From the GO spectrum, we can see several molecular vibrations which correspond to various functional groups attached to the graphene, including hydroxyl (-OH) (1620 cm^{-1}), carbonyl (-C=O) (1726 cm^{-1}), and epoxy groups (C-OC) (1365 cm^{-1}). After the reduction, the number of these functional groups was reduced, resulting in an increase in the transmittance at frequencies associated with the vibrational resonances of these groups [78].

2.3 Scanning Electron Microscopy (SEM)

A Scanning Electron Microscope (SEM) scans a focused beam of electrons over a surface of the sample to create an image. The electrons in the beam interact with the sample, producing various signals that can be used to obtain information about the surface topography and composition [3]. Electrons accelerated at high potentials possess high kinetic energies and when these electrons hit the sample surface, this energy is dissipated as a variety of signals produced by electron-sample interactions.

These signals include secondary electrons (that generate SEM images), backscattered electrons (topography and composition), characteristic X-rays (that are used for elemental analysis). Secondary electrons are valuable for showing morphology and topography on samples and backscattered electrons are most valuable for illustrating contrast in composition in multiphase samples. Figure 2.5 shows the pear-shaped electron beam interaction volume when the sample is bombarded with a beam of electrons with several electron volts of energy [79].

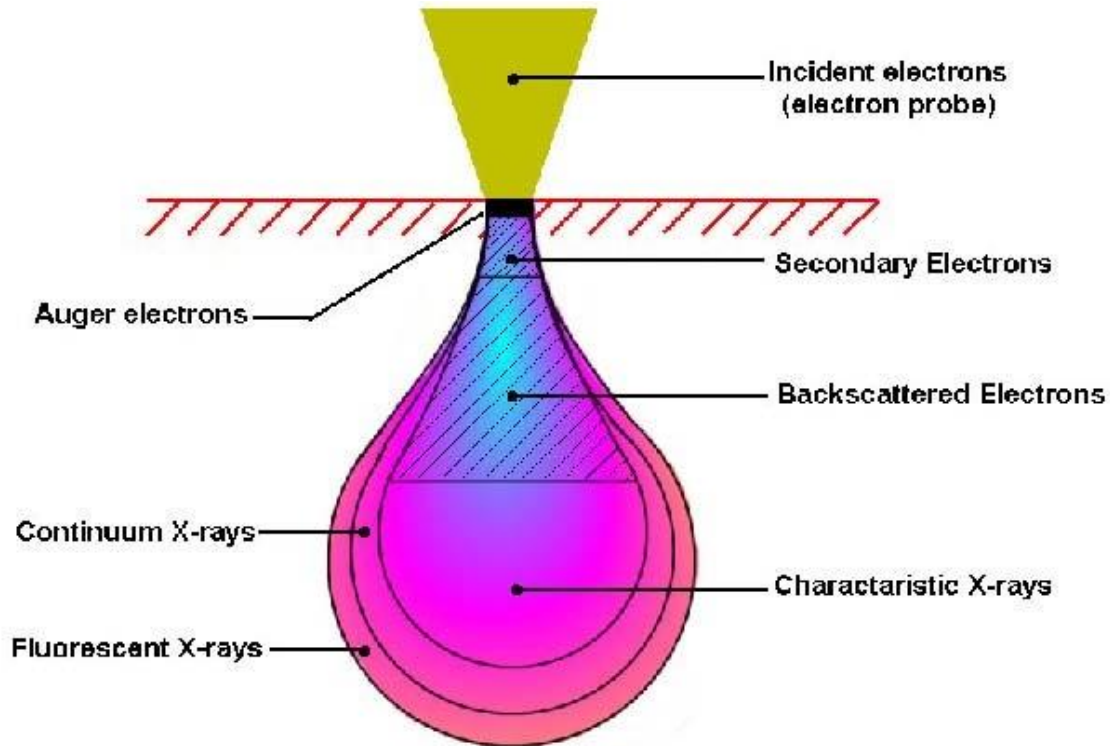


Figure 2.5 Electron beam interaction volume [79]

The SEM consists of the following components:

1. Electron Source (Gun)
2. Column (consists of Electromagnetic lenses and coils for raster scan)
3. Sample holder
4. Detector (Secondary and Backscattered)
5. Computer and display to view the images

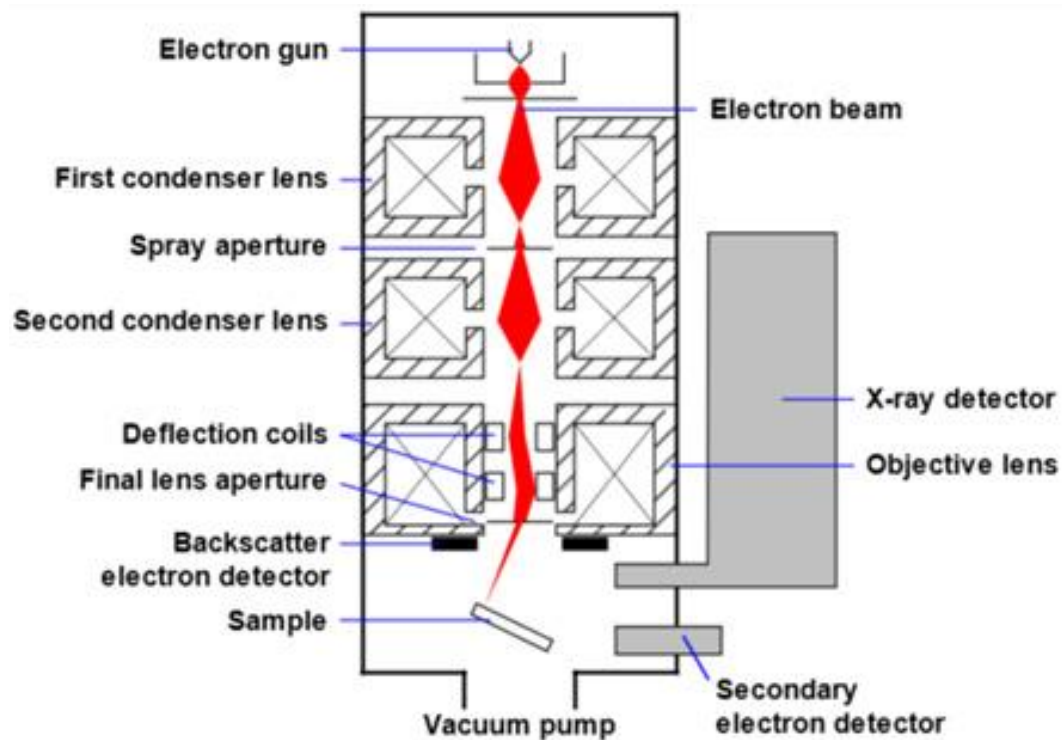


Figure 2.6 Schematic of Scanning Electron Microscope [93].

Electrons produced from the electron gun are accelerated and passed down the column through a combination of apertures, electromagnetic lenses and scanning coils to produce a focused beam of electrons, which hit the surface of the sample. The specimen is mounted on a stage that lies inside a chamber kept at high vacuum. The scan coils are used to control the position of the electron beam in X-Y on the sample surface. This beam scanning or raster-scanning allows the beam to interrogate a defined area on the sample. Several signals such as secondary electrons, backscattered electrons, and x-rays are produced and these signals can then be

detected using an appropriate detector. Figure 2.7 shows the SEM images of GO and rGO films with a resolution of $1\mu\text{m}$ [80].

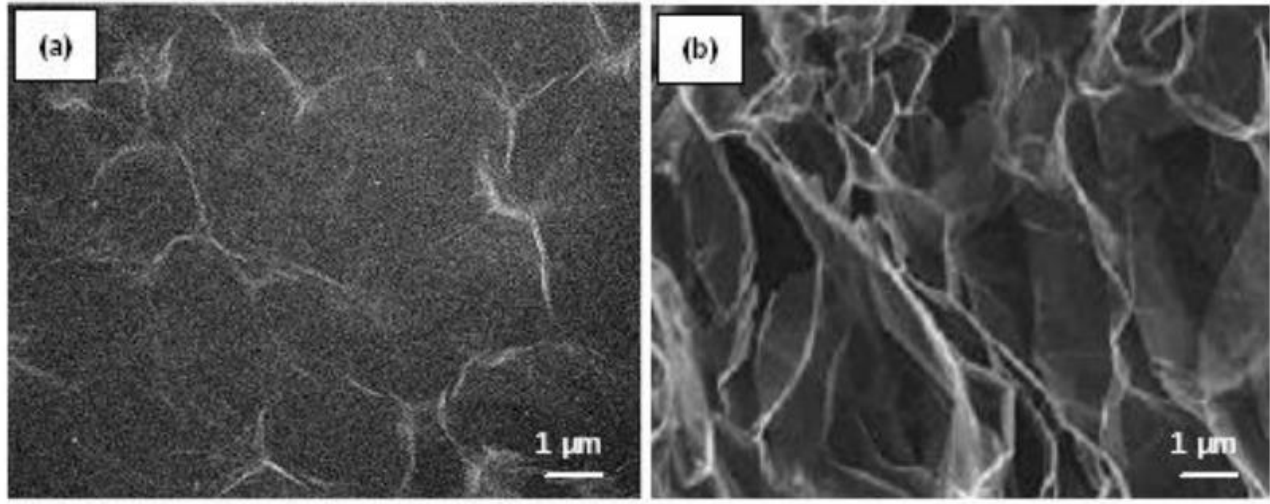


Figure 2.7 SEM images of (a) GO film, (b) rGO film [80].

2.4 Four-Point Probe

The purpose of the four-point probe is to measure the resistivity of material. It can measure either bulk or thin film specimens. The four-point probe consists of four equally spaced tungsten metal tips with finite radius. Each tip is supported by springs to minimize sample damage during probing. The four metal tips are part of an auto-mechanical stage, which travels up and down during measurements. A high-impedance current source is used to supply current through the outer two probes; a voltmeter measures the voltage across the inner two probes to determine the sample resistivity (refer to Figure 2.8) [81]. The typical probe spacing is $\sim 1\text{mm}$.

For a bulk sample, where the sample thickness is greater than probe spacing $t \gg s$, the following expression is used to calculate the bulk resistivity (ρ),

$$\rho = 2\pi s(V/I)$$

Where s = probe spacing; V = voltage measured across the inner probes and I = current given at the outer probes.

In general, the sheet resistance is given by $Rs = \rho/t$ which can be expressed in terms of geometric factor k as

$$Rs = k \left(\frac{V}{I} \right)$$

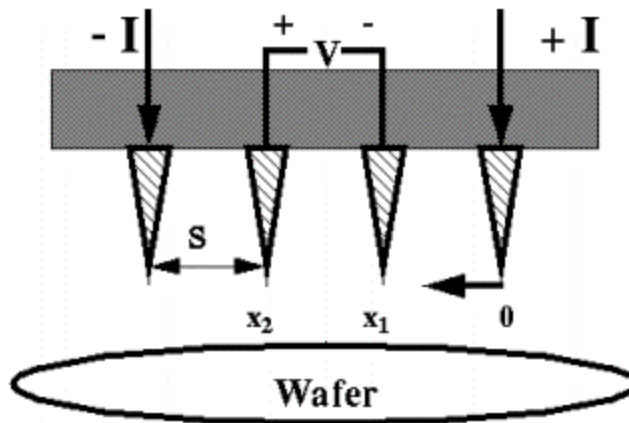


Figure 2.8 Schematic of four point probe configuration [81] .

Chapter 3 : Materials and Methods

3.1 Introduction

The exfoliation of graphite to graphene can be realized either using physical or chemical approaches [82]. Among the various methods, reduction of graphene oxide (GO) to reduced graphene oxide (rGO) is unique and attractive due to its capability of producing single-layer graphene in large scale and at relatively low cost [47]. Furthermore, GO and rGO are solution process able and they can be fabricated or self-assembled into macroscopic materials with controlled compositions and microstructures towards practical applications [83].

3.2 Graphene Oxide Synthesis: Modified Hummer's Method

Graphene oxide was prepared by the oxidation of natural graphite powder (Micro850 from Asbury Graphite Mills Inc., Kittanning, PA, USA) using the modified Hummer's method, i.e. removal of NaNO_3 from the reaction formula, as described in Chapter 1 [84]. Graphite powder (3.0 g) was added to concentrated H_2SO_4 (70 mL) while stirring in an ice bath. Potassium permanganate, KMnO_4 (9.0 g) was added to the reaction mixture slowly to keep the temperature of the suspension lower than 20 °C under vigorous agitation. In the next steps, the reaction system was transferred to an oil bath and vigorously stirred for about 30 minutes at 40 °C. Later, 150 mL of DI water was added to the suspension, and the solution was

stirred for 15 minutes at 95 °C. An additional 450 mL of DI water was added, followed by the slow addition of 15 mL H₂O₂ (30%). This turned the color of the solution from dark brown to yellow and halted the reaction. The reaction system was allowed to rest overnight. Subsequently, the reaction mixture was filtered and washed with 1:10 HCL aqueous solution (250 mL) to remove excess metal ions.

Figure 3.1 shows a schematic flow chart of the all the steps involve in synthesis of GO using modified Hummer's method. Figure 3.2 shows the pictures of the reaction mixture at various stages of the GO preparation.

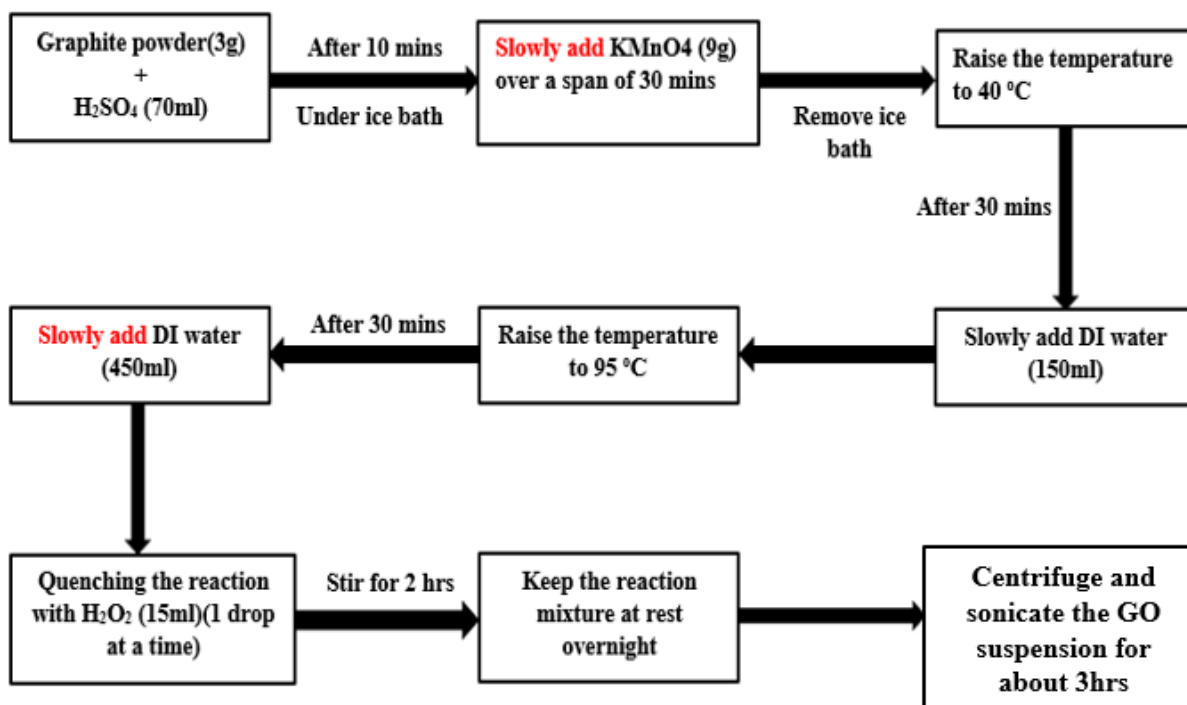


Figure 3.1 Schematic flow-chart of all the steps involved in modified Hummer's method for synthesis of GO.

The resultant graphite oxide aqueous dispersion was then diluted to 1.2 L, stirred overnight and sonicated for 30 minutes to exfoliate it to GO. The GO dispersion was then centrifuged at 3000 rpm for 40 minutes to remove the unexfoliated graphite. After several such centrifugation and sonication steps, GO with a concentration of 6 mg/ml was obtained. The pH of the GO solution was changed to pH = 6 by adding NH_4OH . This pH correction is required to keep the coagulated dispersion stable. It is to be noted that during the modified Hummer's method of oxidation, the graphite particles undergo a significant change in their structure. The overall concentration of oxygen in the particles increases with simultaneous reduction in the carbon content, which eventually increases the oxygen-carbon (O/C) ratio.

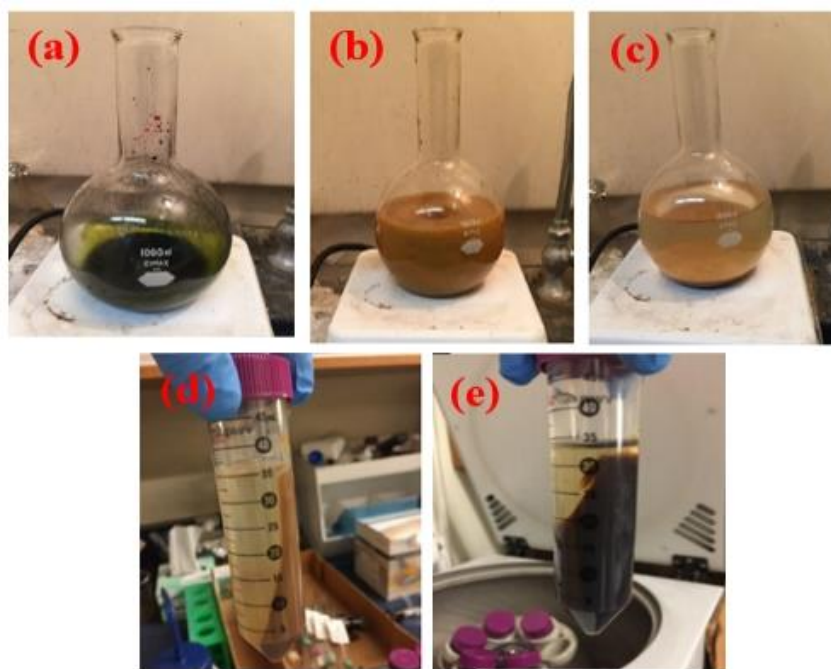


Figure 3.2 (a) Mixture of graphite powder, KMnO_4 , and H_2SO_4 , (b) Reaction mixture upon addition of H_2O_2 and DI water which makes the mixture brown, (c) Reaction mixture left undisturbed overnight, GO solution (d) after centrifugation, and (e) after sonication steps.

A breakage of the carbon sigma bonds to form sp^3 bonding structure is observed during this process of oxidation where oxygenated carbonyl and epoxide groups are formed [85].

3.3 Coagulation of GO suspension with Copper (Cu^{2+}) ions

One of the significant thrusts of recent graphene-based research is to explore changes in physiochemical properties of graphene, graphene oxide, and its derivatives [31]. Divalent cations can be used as cross-linkers between graphene oxide sheets leading to a change in properties such as electrical conductivity, mechanical strength and inter-layer spacing of GO sheets [31] [36]. The chemical interactions occur between the oxygen-containing functional groups and the cations. This interaction can occur either via binding of the cross-linker ions to the carboxylic acid groups at the edges of the GO sheets, or via introduction of the cross-linker ions into the epoxy ring [31]. The two models are shown in Figure 3.3.

In this regard, $CuSO_4$ was used as a precursor to coagulate Cu^{2+} ions in GO dispersion in the present work. GO dispersion with 6 mg/ml concentration was coagulated with different amounts of $CuSO_4 \cdot 5H_2O$; 10, 20, and 50 mM concentrations in aqueous solutions. In this process, the required amount of copper sulfate is added to GO dispersion during continuous stirring to ensure uniform mixing of copper sulfate in GO. The resulting coagulated GO + Cu^{2+} dispersions are

stirred for about an hour and left undisturbed overnight. In this process of coagulation, the electronegative copper ions tend to bond with the more electropositive GO and its functional groups without the help of any binder. Coagulated GO + Cu^{2+} dispersions are washed with water multiple times to remove the SO_4 ions and the excess copper ions that have not bonded with GO and other functional groups.

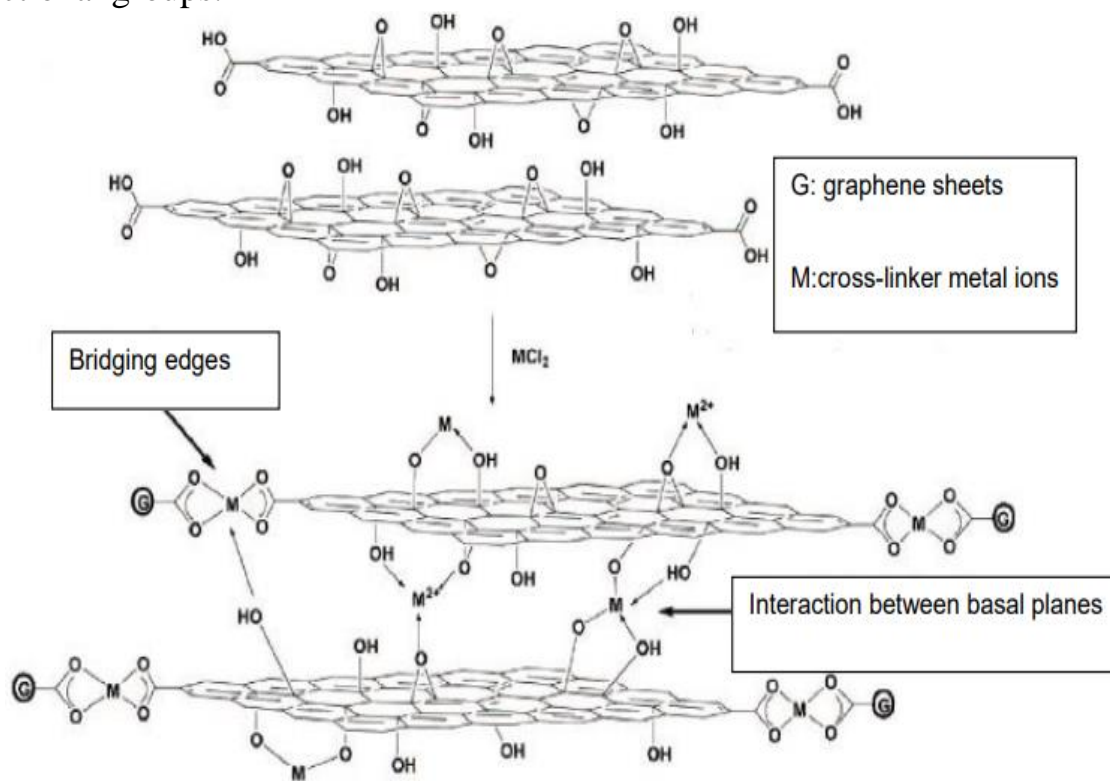


Figure 3.3 The interaction between GO and metal ion cross-linkers [31].

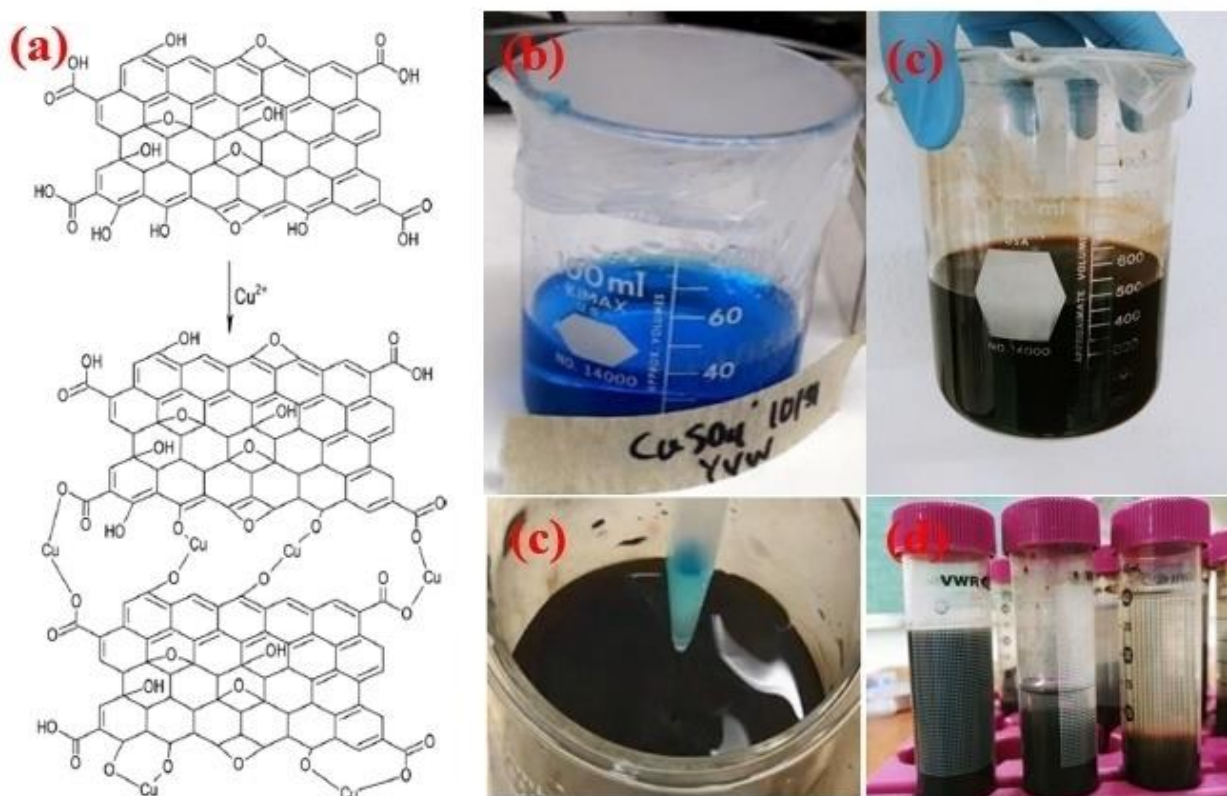


Figure 3.4 (a) Schematic model of the interaction of Cu^{2+} ions with GO and its functional groups, (b) $\text{CuSO}_4 \cdot 5\text{H}_2\text{O}$ in water, (c) pH corrected GO with 6mg/ml concentration, (d) Addition of $\text{CuSO}_4 \cdot 5\text{H}_2\text{O}$ to GO solution under continuous stirring (~ 250 rpm), and (e) GO coagulated with Cu^{2+} ions with different concentration of Cu^{2+} (10, 20, and 50 mM from left).

3.4 Fabrication of GO and GO- Cu^{2+} free standing thin films via doctor blading

Doctor Blading (or tape casting) is a widely used technique to produce thin films over a large area surface. Tape casting was originally developed during 1940's as a method of forming thin sheets of piezoelectric materials and capacitors and is now an accepted precision coating method [86]. In a typical doctor blading process, well-

mixed slurry consisting of a suspension of particles along with other additives like binders and dispersants is placed on the substrate beyond the doctor blade. When a constant relative motion is applied between the blade and the substrate, the slurry spreads uniformly on the substrate to form a thin layer, which, upon drying, gives a thin film. This film can be peeled off the substrate using a razor blade resulting in a freestanding film. The doctor blade can operate at speeds up to several meters per minute and is suitable to coat substrates with a wide range of wet-film thicknesses ranging from 20 to several hundred microns.

Doctor Blading can be also used in combination with a reservoir. The thin layer (wet) is formed by a doctor blade that is either stationary when used with a moving substrate, or by a frame that moves along a stationary casting surface. Figure 3.5 shows the schematic diagram of doctor blade and thickness control by changing the gap between the blade and the substrate.

In the present study, as-prepared GO and GO + Cu²⁺ solutions with a GO concentration of 6 mg/ml and various Cu²⁺ concentrations of 10, 20, and 50 mM were used in the doctor-blade coating process to form free standing thin films. The solutions were spread onto a glass substrate (pre-cleaned with ethyl alcohol and acetone) and the doctor blade was moved across the solution on the glass substrate with a gap of 50 µm between the blade and the substrate. The coated film (wet) was allowed to dry in ambient conditions for 24 hours and peeled off from the glass films

substrate using a razor blade to obtain free standing GO and GO + Cu²⁺ films of 50 μm thickness. The gap between the blade and the substrate can be varied to form two to several micrometers used to set the blade height (see Figure 3.6 b) should be kept at same level to ensure optimum thin film thickness.

To support the examination of Cu effects in GO film formation and subsequent reduction, three, 1000ml batches of GO were synthesized and used for film production. A suite of thirty-six specimens were used to furnish four specimens for each parameter condition studied over a 2-D matrix of sample preparation

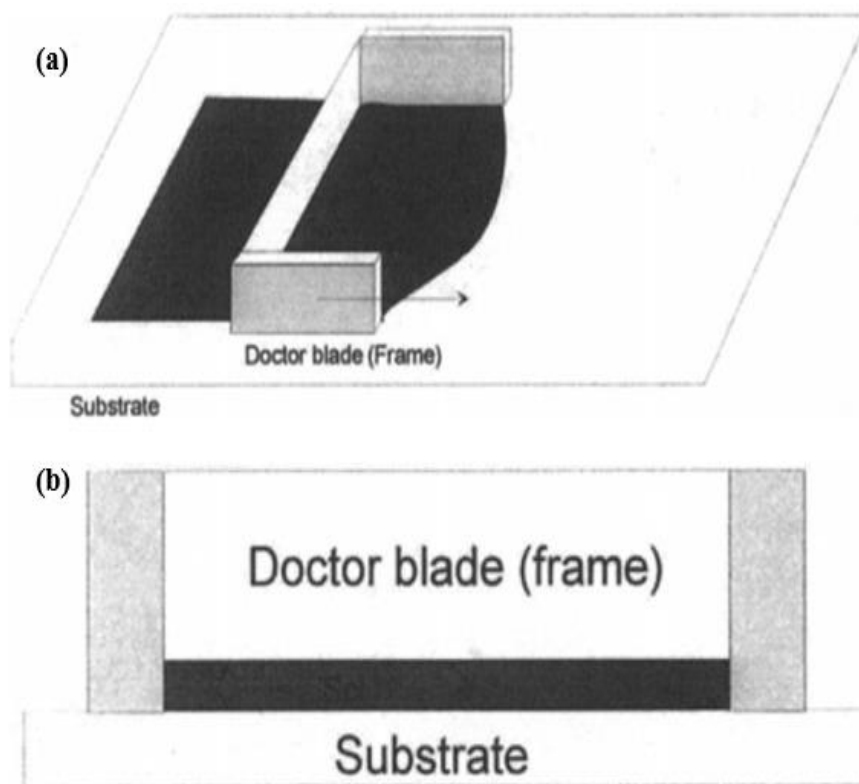


Figure 3.5 (a) Principle of doctor blading using a frame with reservoir of coating material which is moving relatively to the surface, (b) Thickness control of the thin layer by the gap between the frame (blade) and the substrate [86].

conditions, i.e. varying copper concentration (10, 20, and 50 mM) and film thickness (25, 50, and 100 μm).

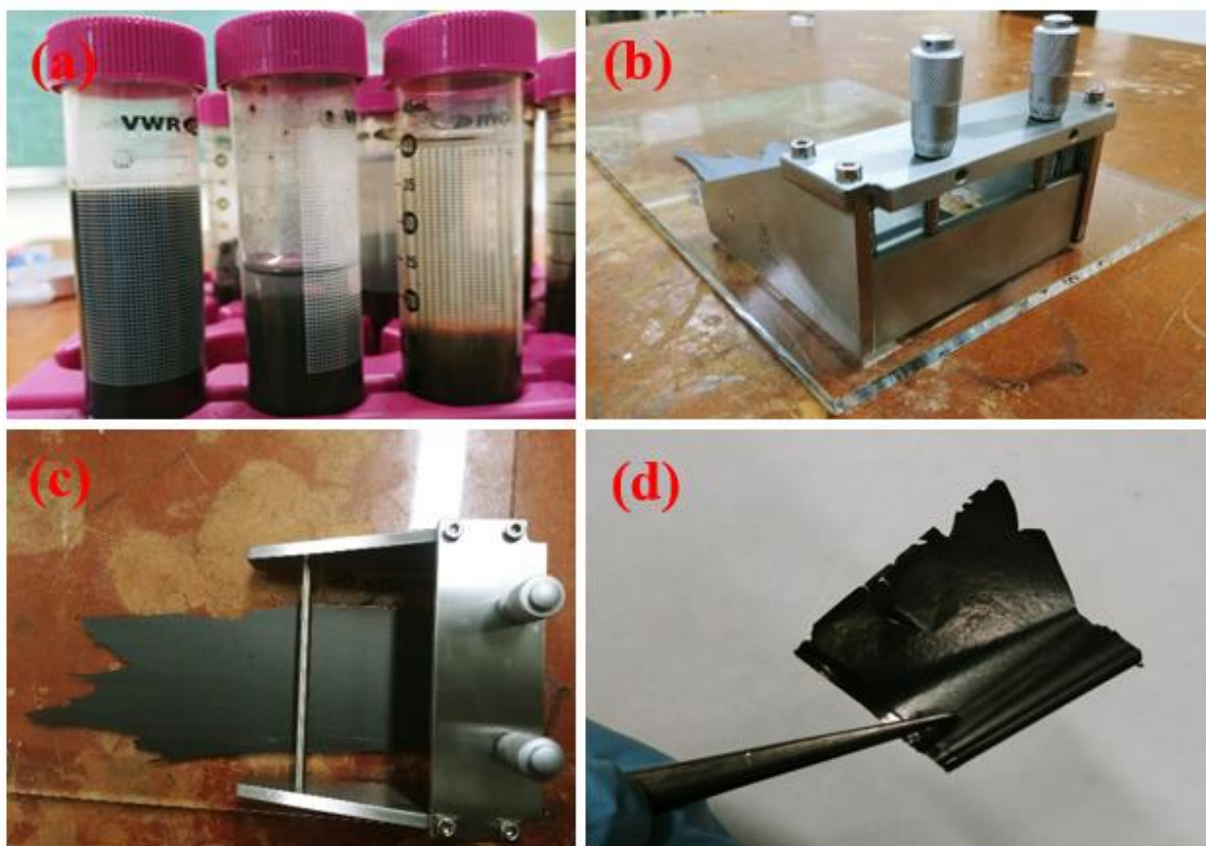


Figure 3.6 (a) Different of concentrations (10, 20, and 50 mM) of Cu^{2+} in GO dispersion (from left side), (b) Side view of a doctor blade coating process on a glass substrate, (c) Top view of a doctor blade coating process, and (d) Free standing film (GO + Cu^{2+} film of thickness 50 μm) obtained from doctor blade coating process (after peeling the film from the substrate).

3.5 Low temperature thermal annealing of GO and GO + Cu²⁺ thin films

Thermal reduction (thermal annealing) is a conventional method for the reduction of GO to enhance its electrical conductivity by the removing the oxygen-containing functional groups and regaining sp³ hybridization. This reduction leads to an evaporation of the intercalated water and evolution of gases produced by thermal pyrolysis of the oxygen-containing functional groups. A schematic showing the ideal reduction of GO into reduced graphene oxide is shown in Figure 3.7, where all the oxygen-containing functional groups are removed and the π network has been completely restored. This annealing was carried out in a vacuum oven using a mechanical vacuum pump. GO and GO + Cu²⁺ free standing thin films were sandwiched between two glass slides to reduce the wrinkling often observed and associated with volume reduction as the oxide functional groups are removed during thermal treatment. The oven was preheated to the required process temperature (170

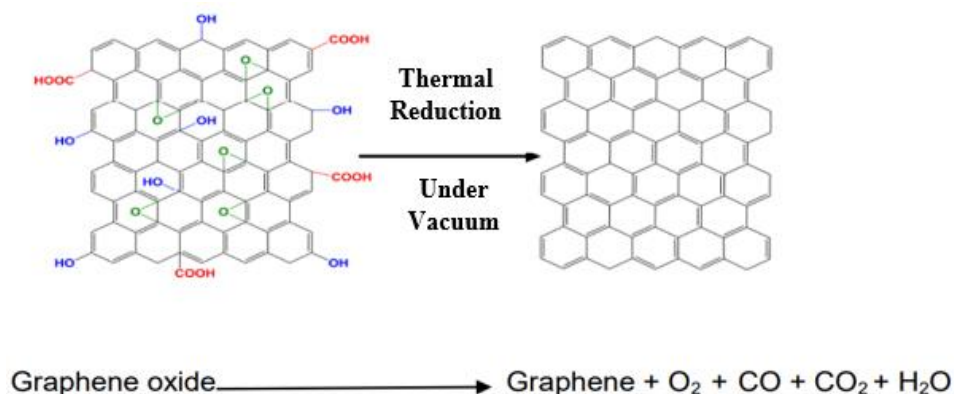


Figure 3.7 Schematic of the reduction of graphene oxide into reduced graphene oxide by thermal treatment [89].

°C) before the samples were placed in the oven. Once the oven was sealed, the mechanical vacuum pump was used to keep the annealing chamber at $\sim 10^{-3}$ Torr. Annealing is performed for 90 minutes before cooling down under vacuum (30 minutes) to the room temperature. The thermal annealing conditions for GO and GO + Cu²⁺ freestanding thin films reduction are shown in the Table 3.1. There was change in the color of the GO + Cu²⁺ film and the film became more brittle after the thermal reduction which can be related to the removal of functional groups and some carbon content from the film. This is evident from the Figure 3.8 (c).

Table 3-1 Thermal reduction conditions for GO and GO + Cu²⁺ free standing thin films

Process Parameter	Process Condition
Temperature (°C)	170 °C
Pressure (Torr)	$\sim 10^{-3}$ Torr
Duration (Minutes)	90 minutes

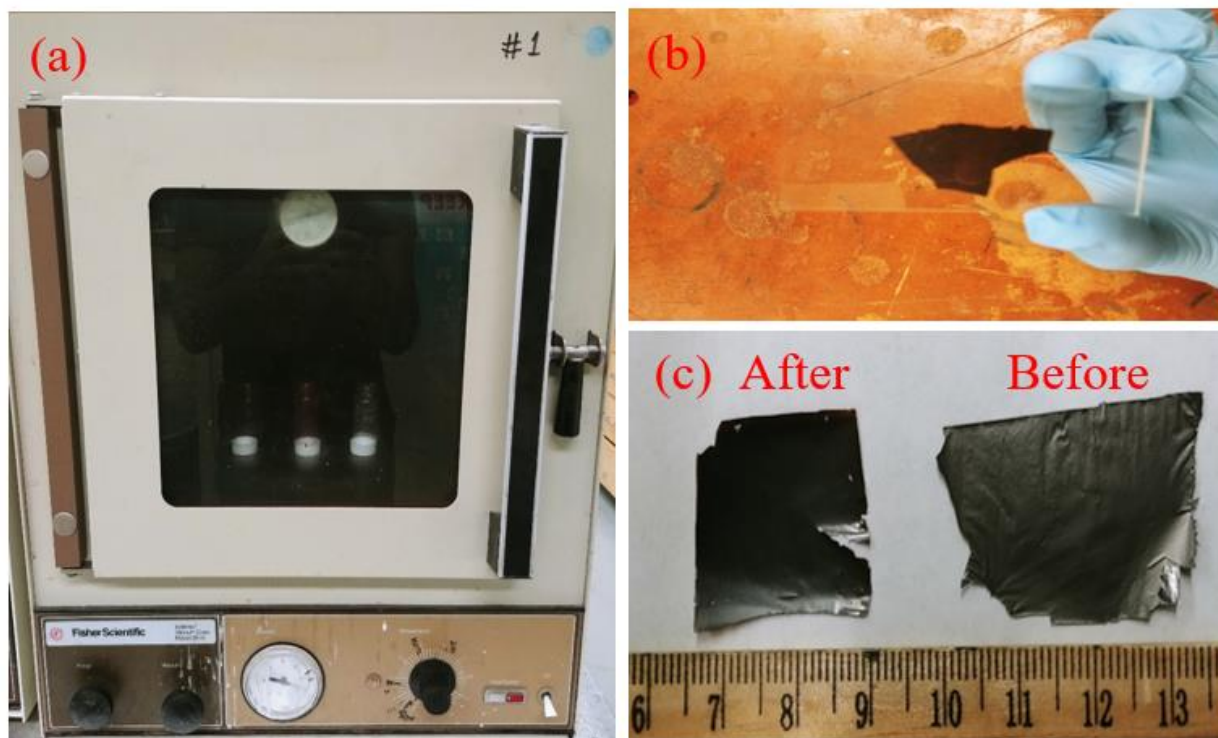


Figure 3.8 (a) Vacuum oven with temperature and vacuum control (Courtesy: Prof. D.A. Loy's lab) (b) GO + Cu^{2+} 50 μm thin film sandwiched between two glass slide before the thermal reduction (c) GO + Cu^{2+} free standing film after and before the thermal reduction at 170 $^{\circ}\text{C}$ for 90 minutes.

3.6 Laser reduction of GO + Cu^{2+} free-standing thin films

Laser reduction of GO has emerged as one of the promising methods for producing high-quality reduced graphene oxide and several groups have been investigating this photo reduction approach. The laser reduction experimental setup used in the current effort consists of a diode laser (Laserglow Technologies), beam steering and optics setup, 1 x 1 cm^2 area mask, and free-standing thin film to be reduced. A picture of the experimental setup is shown in Figure 3.9. The diode laser

has a wavelength of 405 nm and operates in continuous-wave (CW) mode. The laser beam is directed towards the freestanding thin film with the help of a beam steering setup and a concave lens to obtain a collimated beam. A final 1 cm x 1 cm square mask restricts the specimen area exposed to the beam. The beam profile at the thin film (after the mask) was obtained by measuring the power transmitted through a 50 μm wide slit at 15 regular positions across the beam along both primary axes of the square mask. Variation in the beam power over the 1 cm x 1 cm mask area was found to be $\pm 4.20 \mu\text{W}$.

A fluence-dependent assessment of the photo response of the GO-Cu material was pursued. Fluence was varied using two approaches, 1. Variation in beam intensity with a constant exposure time and, 2. Variation in exposure time while maintaining a constant beam intensity.

In the first study, GO + Cu²⁺ (with 50 mM Cu²⁺) thin films are irradiated with intensities of 0.08, 0.25, 0.42, and 0.5 mW/cm² for 5 minutes. This resulted in accumulated fluences of 25, 75, 125, and 150 mJ/cm² respectively. In the second study, the GO + Cu²⁺ (50 mM Cu²⁺) thin films were irradiated with a constant intensity beam (0.5 mW/cm²) for time periods of 5, 10, 20, 40, 80 and 160 minutes. The associated accumulated fluences were 150, 300, 600, 1200, 2400, 4800 mJ/cm².

The effect of the photo exposures was evaluated using the FT-IR spectra collected after photo processing. In both fluence studies, spectra were collected iteratively after each successive photo exposure to assess the cumulative effect of fluence on the film structure.

Figure 3.9 a, b shows the optical exposure experimental set-up. Figure 3.9c includes the representative beam profile at the sample.

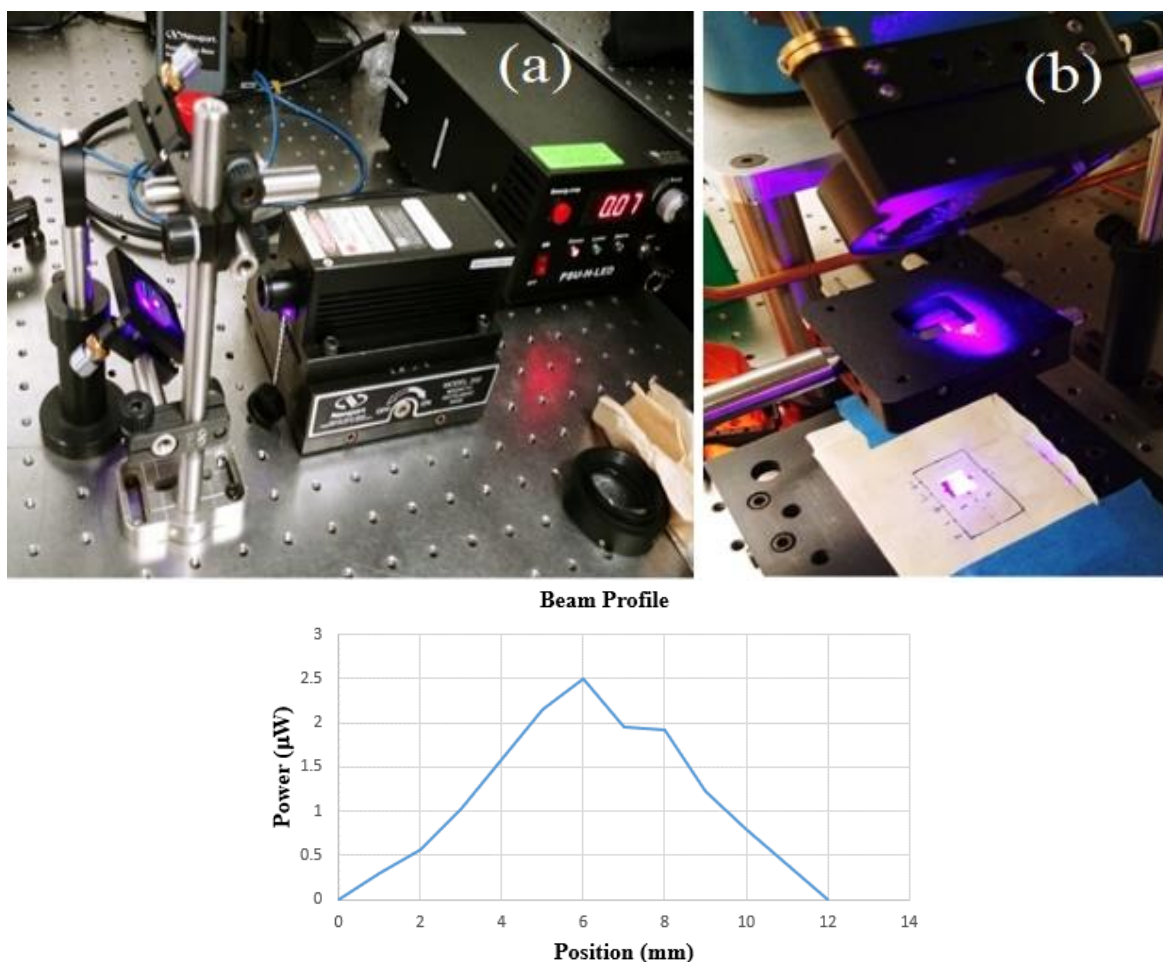


Figure 3.9 (a) 405 nm CW diode laser with the beam steering setup and a concave lens of focal length +75 mm, (b) GO + Cu²⁺ (with 50 mM Cu²⁺) irradiated with a 1 x 1 cm² mask. (c) Plot showing beam intensity profile after the mask with power on y-axis and position on x-axis.

Chapter 4 : Results & Discussion

A suite of characterization techniques was used to evaluate the effects of post-deposition processing (i.e. thermal reduction and photo reduction) on the chemical composition, morphology, optical, and electrical properties of the doctor-blade-produced films. These techniques included X-ray photoelectron spectroscopy (XPS), scanning electron microscopy and electron dispersive spectroscopy (SEM/EDS), Fourier transform infrared spectroscopy (FTIR), and four-point probe measurements. A description of these techniques was provided in the background section (Chapter 2).

4.1 Chemical analysis using XPS

XPS spectra were collected with a Kratos 165 Ultra-Photoelectron Spectrometer using an Al K α X-ray source. The slot aperture of the x-ray beam was set to 700 X 300 μm . XPS is often used as a technique for confirming the reduction of GO + Cu²⁺ hybrid thin film. XPS is capable of quantitative measurement of material composition and of elucidating the chemical environment surrounding atoms by measuring core level shifts.

Figures 4.1 and 4.2 below illustrate the XPS spectra collected from the GO + Cu²⁺ (with a Cu²⁺ concentration of 50 mM) film before (Figures 4.1 a and 4.2 a) and after (Figures 4.1 b and 4.2 b) low temperature thermal reduction in vacuum ($\sim 10^{-3}$

Torr). Figures 4.3 (a), and (b) show the XPS spectra of Cu2p before and after the reduction in GO + Cu²⁺ (with a Cu²⁺ concentration of 50 mM). It should be noted that this data is only representative of the surface of the sample as the escape depth of X-ray photoelectrons at these energies is about ~10 nm.

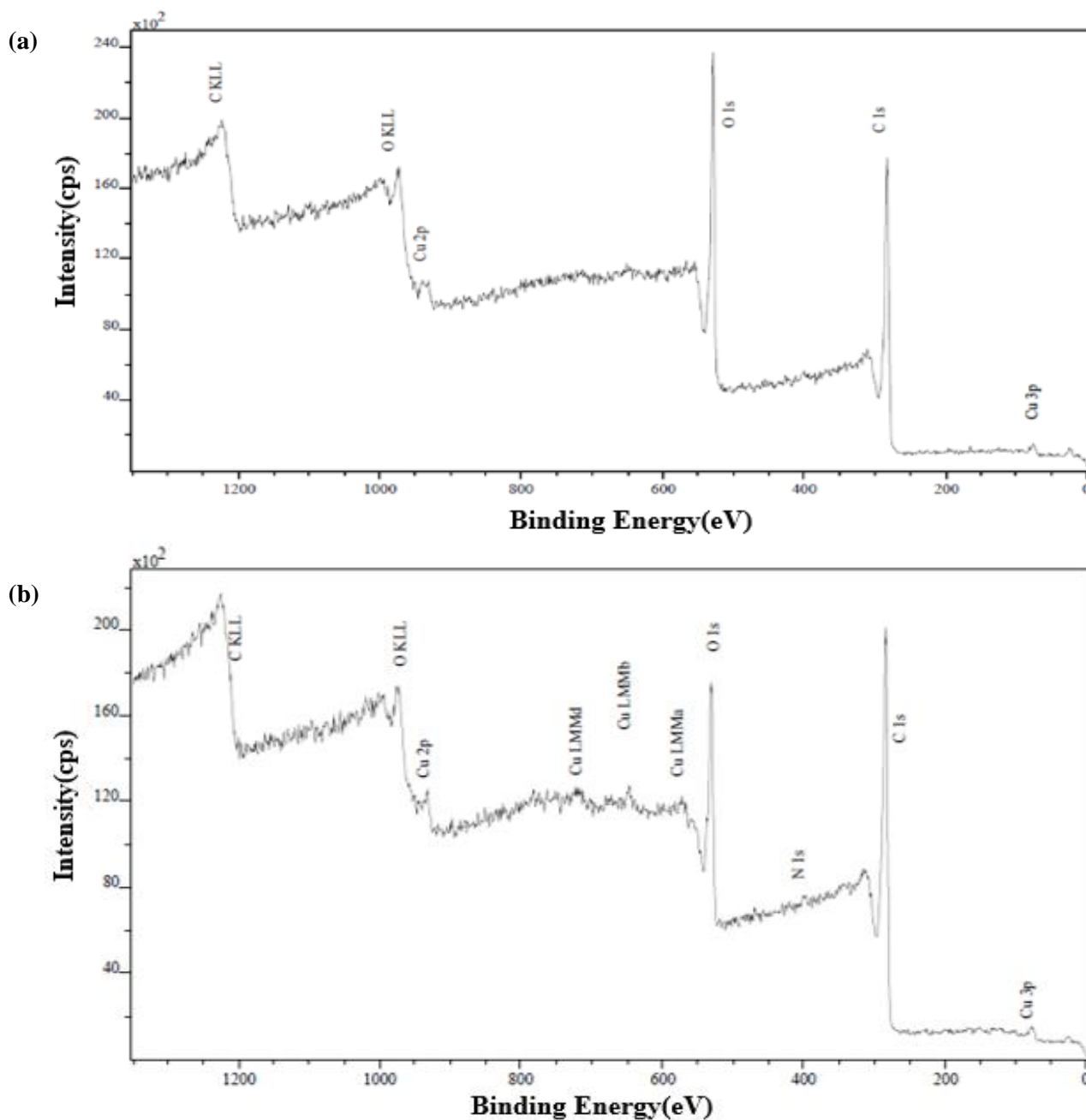


Figure 4.1 XPS survey spectra of GO + Cu²⁺ before (a) and after (b) thermal reduction in vacuum at 170 °C for about 90 minutes. GO-Cu²⁺ before reduction has a C/O ratio of ~ 0.75. After the low temperature thermal reduction, the oxygen content decreased and the C/O ratio increased to ~1.2.

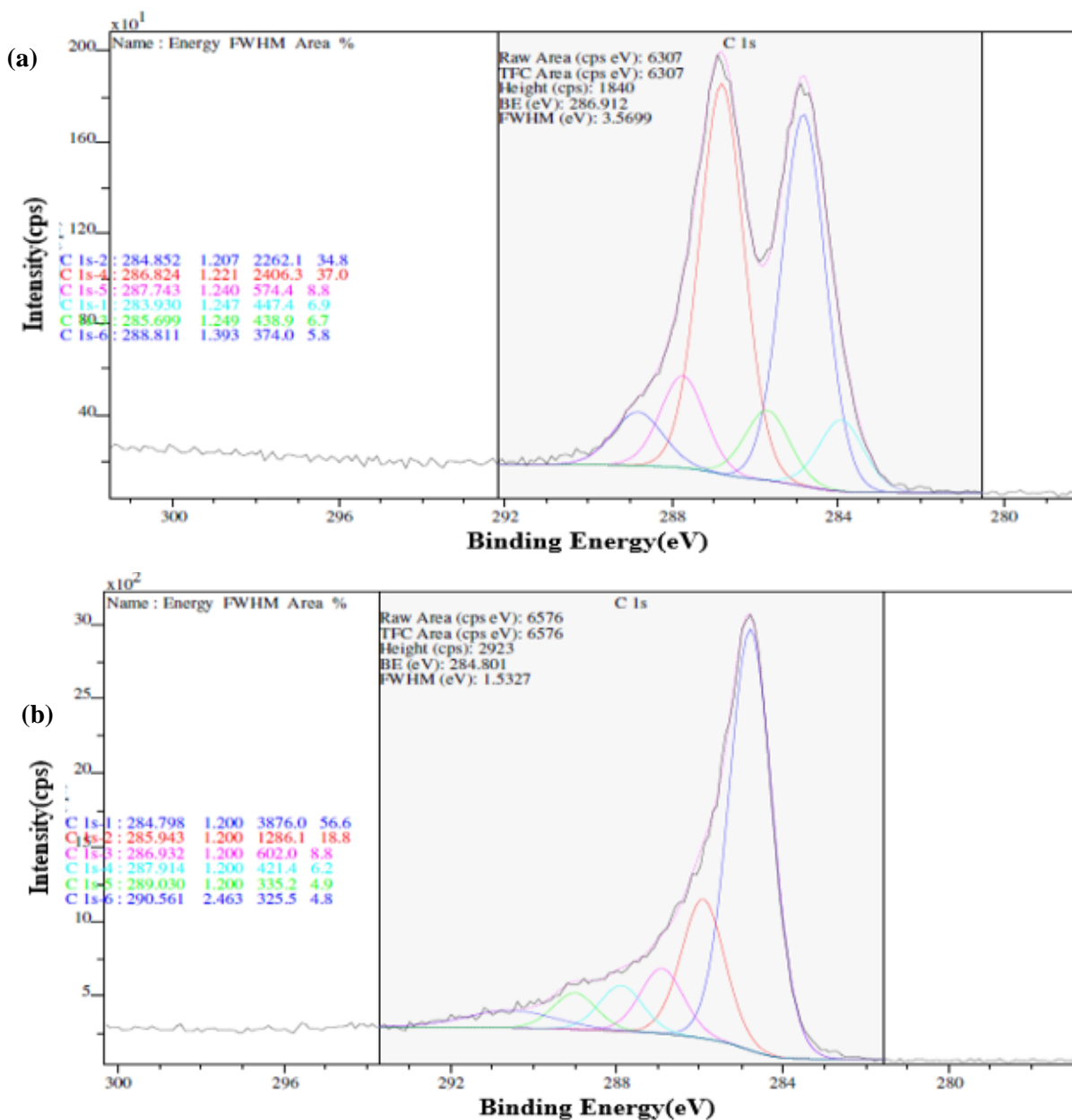


Figure 4.2 XPS C1s spectra of GO + Cu²⁺ before (a) and after (b) low temperature thermal reduction in vacuum at 170 °C for 90 minutes. Before reduction, the C1s peak analysis of the unreduced GO+Cu²⁺ films reveal the presence of oxygen containing functionalities in the form of epoxy, hydroxyl, and carbonyl groups. After thermal reduction, the peaks associated with the oxygen containing functionalities are diminished, and the predominance of the sp² hybridized carbon peak (blue curve peak position at ~ 284.798 eV) confirms graphene formation.

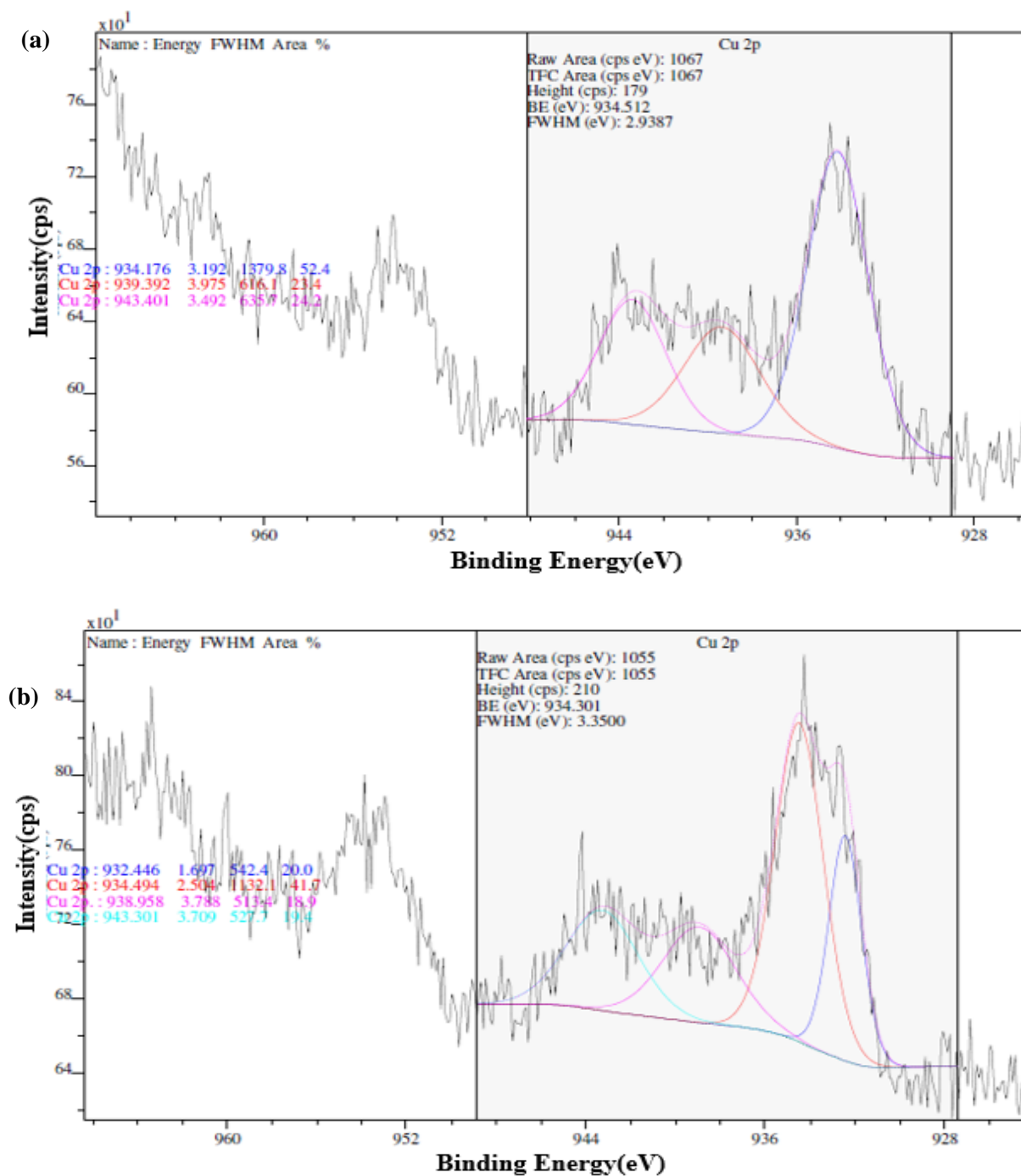


Figure 4.3 XPS Cu2p spectra of GO + Cu²⁺ before (a) and after (b) low temperature thermal reduction in vacuum at 170 °C for 90 minutes. Before reduction, the Cu2p peak analysis of the unreduced GO + Cu²⁺ film reveals the presence of copper ions (~934.4 eV) and their predominant oxidation state is 2+. After reduction, the peaks corresponding to Cu2p remained unchanged and the predominant oxidation state of copper was 2+.

The unreduced GO + Cu²⁺ (50 mM Cu²⁺) film (Figure 4.1 a), as expected, has dominant carbon, oxygen features, and the presence of copper is from the coagulation of Cu²⁺ in GO. From the XPS survey spectrum, it is understood that the carbon (C1s) peak has a binding energy of ~ 288 eV; oxygen (O1s) peak appears at ~ 533 eV. The corresponding binding energy of Cu2p was ~934.176 eV and the other peaks at ~939.392 eV and ~943.401 eV are related to the Cu²⁺ satellite peaks. The C/O ratio was determined based on the ratio of carbon (C1s) and oxygen (O1s) peaks shown in the survey spectrum (Figure 4.1 a, b). The C/O ratio depends on the functionalization of GO and reduction of the same into reduced form.

The C/O ratio of unreduced GO + Cu²⁺ (50 mM Cu²⁺) films is ~ 0.7. Curve fitting of the C1s peak (Figure 4.2 a) reveals the presence of oxygen containing functionalities in the form of epoxy, hydroxyl, and carbonyl groups. After the thermal reduction, a drastic change for oxygen is observed (Figure 4.2 b). The oxygen content was decreased and, in turn, the C/O ratio reaches ~ 1.2. Curve fitting of the C1s peak in the thermally reduced GO + Cu²⁺ (50 mM Cu²⁺) film (Figure 4.2 b) confirms a predominance of sp² hybridized carbon, indicating the formation of graphene. However, a contribution from the functional groups is observed even after the reduction.

The spectra of GO + Cu²⁺ (with 50 mM of Cu²⁺) shows an intense peak at ~ 284.7 eV, attributed to carbon with sp² and sp³ hybridization accompanied by some

shoulders at higher binding energies due to the presence of oxygen linkages. The sample also shows a second intense peak at ~ 286.9 eV, ascribed to hydroxyl and epoxy groups, and less intense contributions of carbonyl/quinone (~ 287.9 eV) and carboxyl (~ 289.0 eV). The oxygen speciation in the GO + Cu²⁺ (50 mM Cu²⁺) sample is in agreement with the model of Lerf- Klinowski concerning highly oxidized graphitic structures [87].

The spectrum of rGO + Cu²⁺ (with 50 mM Cu²⁺) shows an intense peak at ~ 284.7 eV attributed to carbon with sp² hybridization. The C1s spectrum of rGO + Cu²⁺ consists of a peak at 284.7, 285.9, 286.9, 287.9, 289.03, and 290.5 eV assigned to C-C, C-O, C=O, O-C-O, O=C-OH, and π - π^* transition in aromatic systems, respectively.

The presence of Cu²⁺ in GO + Cu²⁺ (with 50 mM of Cu²⁺) can be confirmed from the XPS survey spectrum of GO + Cu²⁺ before and after reduction (Figure 4.1 a and b). In the unreduced GO + Cu²⁺ film, copper ions were present in 2+ oxidation state predominantly. Upon thermal reduction, there was no change observed in the XPS spectra of Copper ions. Curve fitting of the Cu2p in the thermally reduced GO + Cu²⁺ film reveals that copper is predominantly present in 2+ oxidation state and corresponding binding energy is ~ 934.494 eV.

4.2 Morphology and elemental analysis using SEM & EDS

SEM images and EDS spectra were collected using the FEI Helios electron microscope. SEM secondary electron images were used to study the morphology changes in GO + Cu²⁺ thin films before and after the reduction (thermal and laser reduction). EDS spectra and elemental maps were also examined before and after the reduction of films. Electron imaging was particularly useful in the studying the morphology changes with reduction in films containing different Cu concentrations.

Figure 4.4 a & b illustrate the morphology changes in GO thin films of thickness 50 μm before and after coagulation of Cu²⁺ ions (50 mM), respectively. These SEM images revealed stacked, wrinkled and layered GO sheets, due to the local folding arising from aggregation in the presence of divalent metal ions (Cu²⁺). Figure 4.5 a & b contain the SEM images of thermally reduced GO + Cu²⁺ (50mM Cu²⁺ concentration and 50 μm thickness) and laser reduced GO + Cu²⁺ (50 mM Cu²⁺) of similar concentration and thickness, respectively. These images show that thermal reduction appears induced more defects and increased surface damage of the GO + Cu²⁺ thin film than the laser reduced thin film.

In comparison, Figure 4.6 contains the SEM image of reduced GO film (50 μm) (i.e. no Cu addition) via thermal reduction and the EDS spectra showing the elemental composition of the thin film with elemental mapping of carbon and

oxygen. These images (and corresponding compositional estimates) reveal that some amount of carbon and oxygen was removed from the thin film, which is due to the thermal reduction. EDS spectra shows that there has been contamination in the thin film and which could have occurred during synthesis of GO (Improper cleaning of magnetic stir bars and glassware used for other materials) and coagulation of Cu^{2+} in GO. Sonication of the GO and GO + Cu^{2+} dispersions and improper cleaning of glass substrates used for fabrication of free standing films might be other reasons of contamination.

Figure 4.7 shows the SEM image and EDS spectra of thermally reduced GO + Cu^{2+} thin film with 10 mM Cu^{2+} concentration. Figure 4.8 a & b shows the SEM image and EDS spectra of thermally reduced GO + Cu^{2+} thin film with 20 mM concentration of Cu^{2+} . Figure 4.9 (a) & (b) illustrate the SEM image and EDS spectra of thermally reduced GO + Cu^{2+} thin film with 50 mM Cu^{2+} concentration. From the EDS images of above-mentioned figures, it is evident that Cu^{2+} ions are uniformly distributed in the thermally reduced thin film with weight percent of 6.53, 7.09, and 9.02.

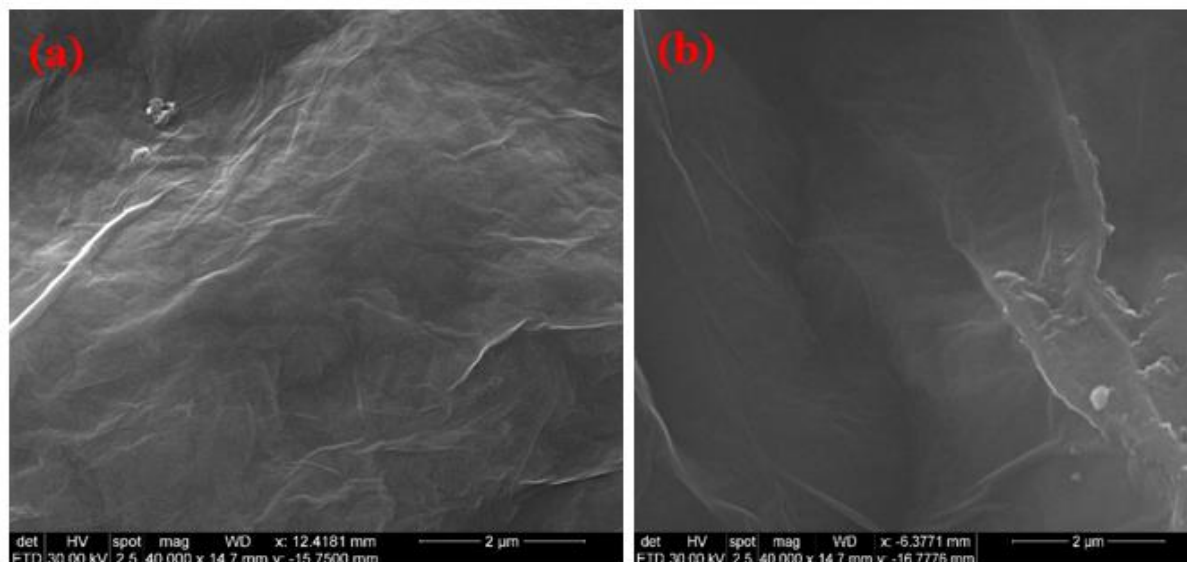


Figure 4.4 (a) SEM image of GO film (50 μm) (b) SEM image of GO coagulated with 50 mM Cu^{2+} (50 μm thick).

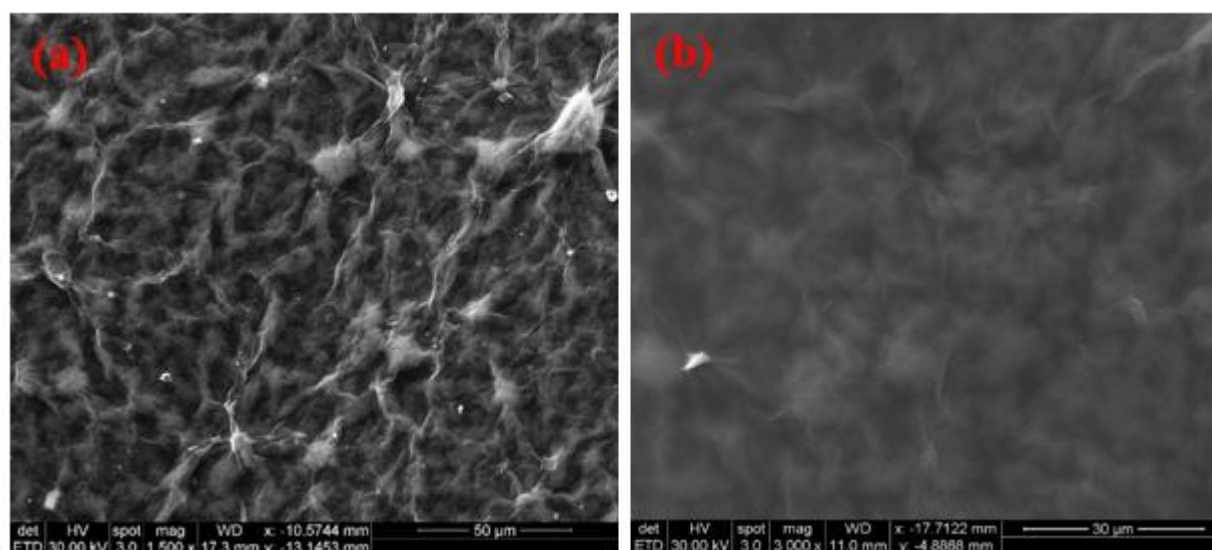


Figure 4.5 Typical SEM image of thermally reduced GO + Cu^{2+} (50 μm) film at 170 $^{\circ}\text{C}$ for 90 minutes under vacuum (b) SEM image of a laser reduced GO + Cu^{2+} (50 μm) film with a fluence of 75 mJ/cm^2 .

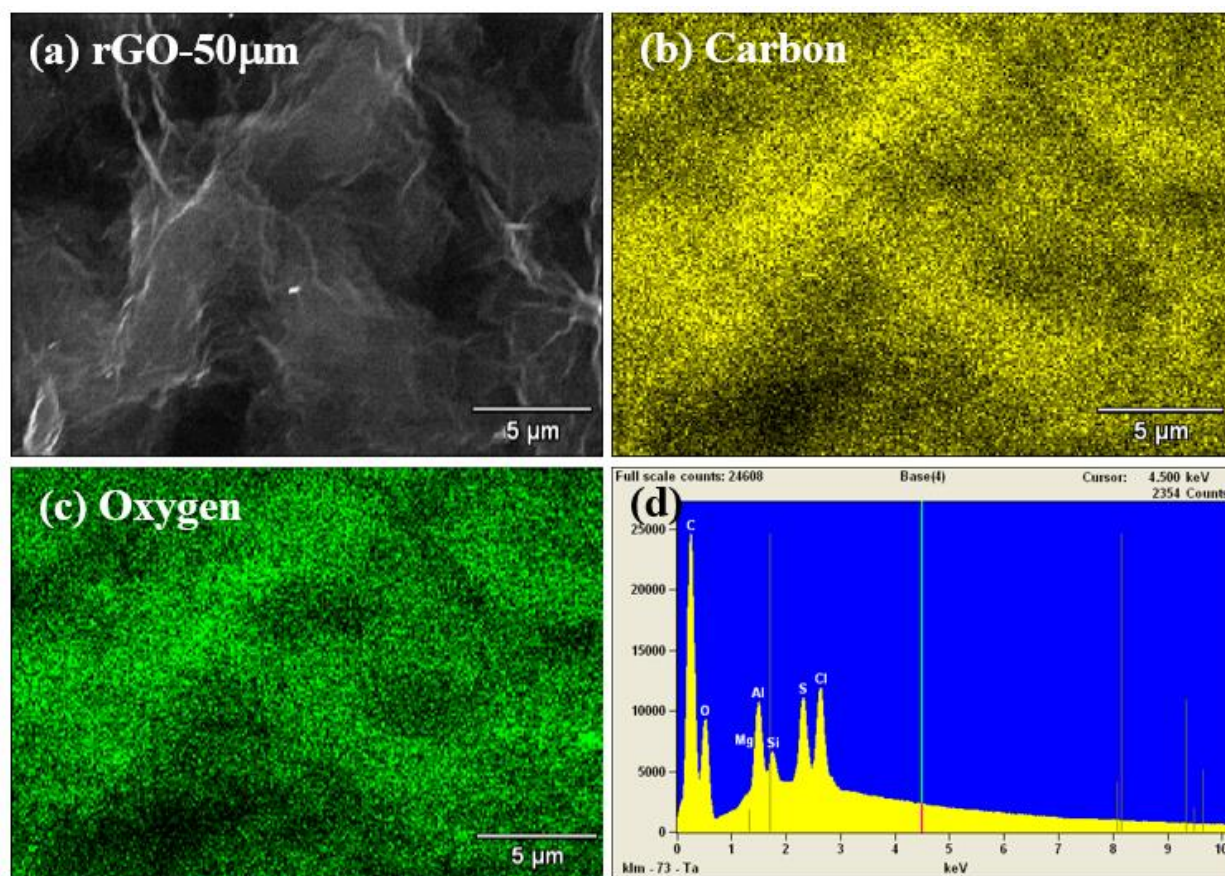


Figure 4.6 (a) SEM image of reduced GO film (50 μm) via low temperature thermal reduction (b) Distribution map of carbon over the scanned area of rGO film. (c) Distribution map of oxygen over the scanned area of rGO film (d) EDS spectrum of rGO film (50 μm) reduced via thermal reduction.

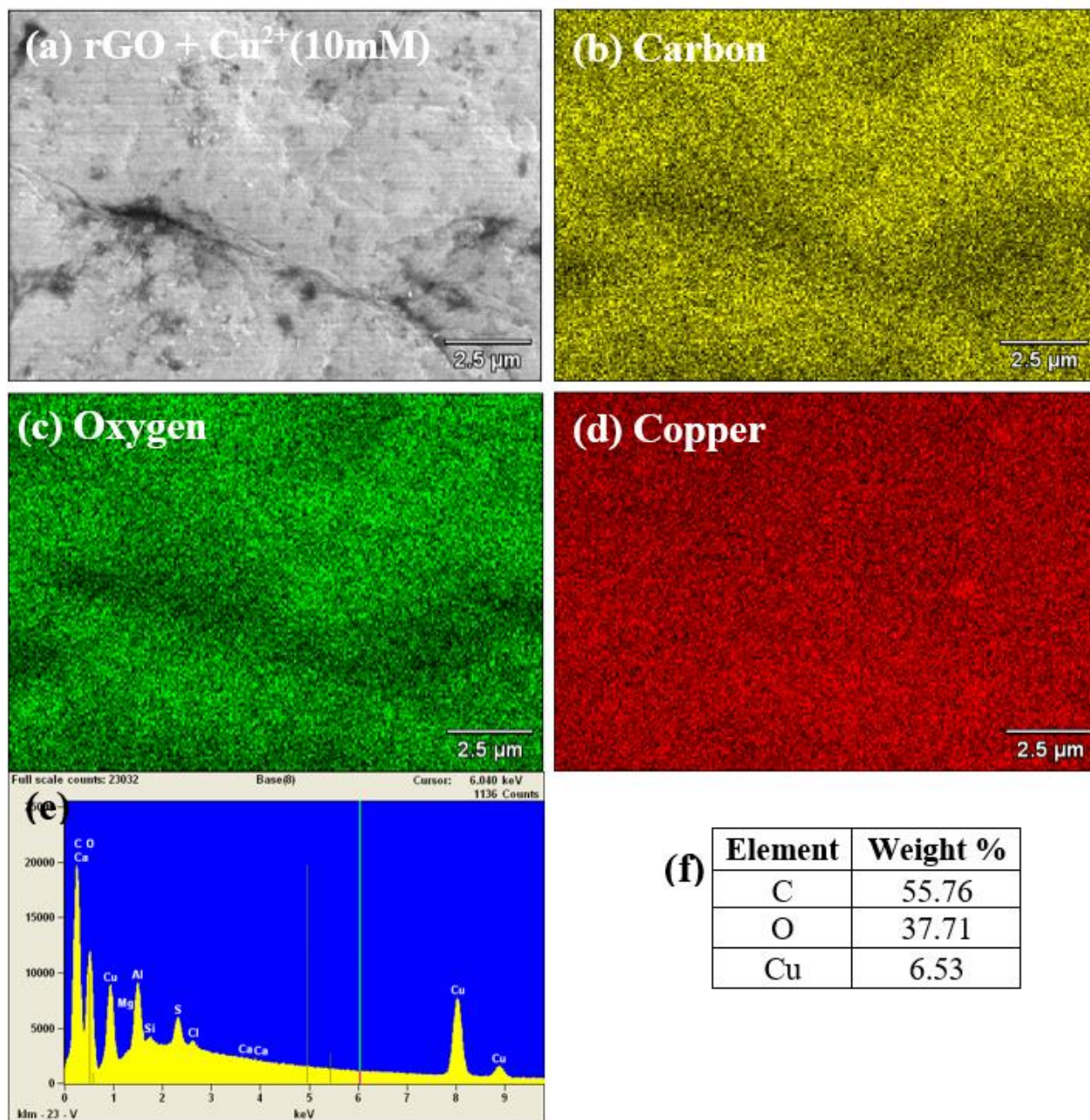


Figure 4.7 (a) SEM image of reduced GO + Cu²⁺ film (50 μm) with 10 mM CuSO₄ via low temperature thermal reduction (b) Distribution map of carbon over the scanned area of reduced GO + Cu²⁺ film. (c) Distribution map of oxygen over the scanned area of reduced GO + Cu²⁺ film (d) Distribution map of copper over the scanned area of reduced GO + Cu²⁺ film (e) EDS spectrum of reduced GO film (50 μm) reduced via thermal reduction (f) Elemental composition of reduced GO + Cu²⁺ (10 mM) film.

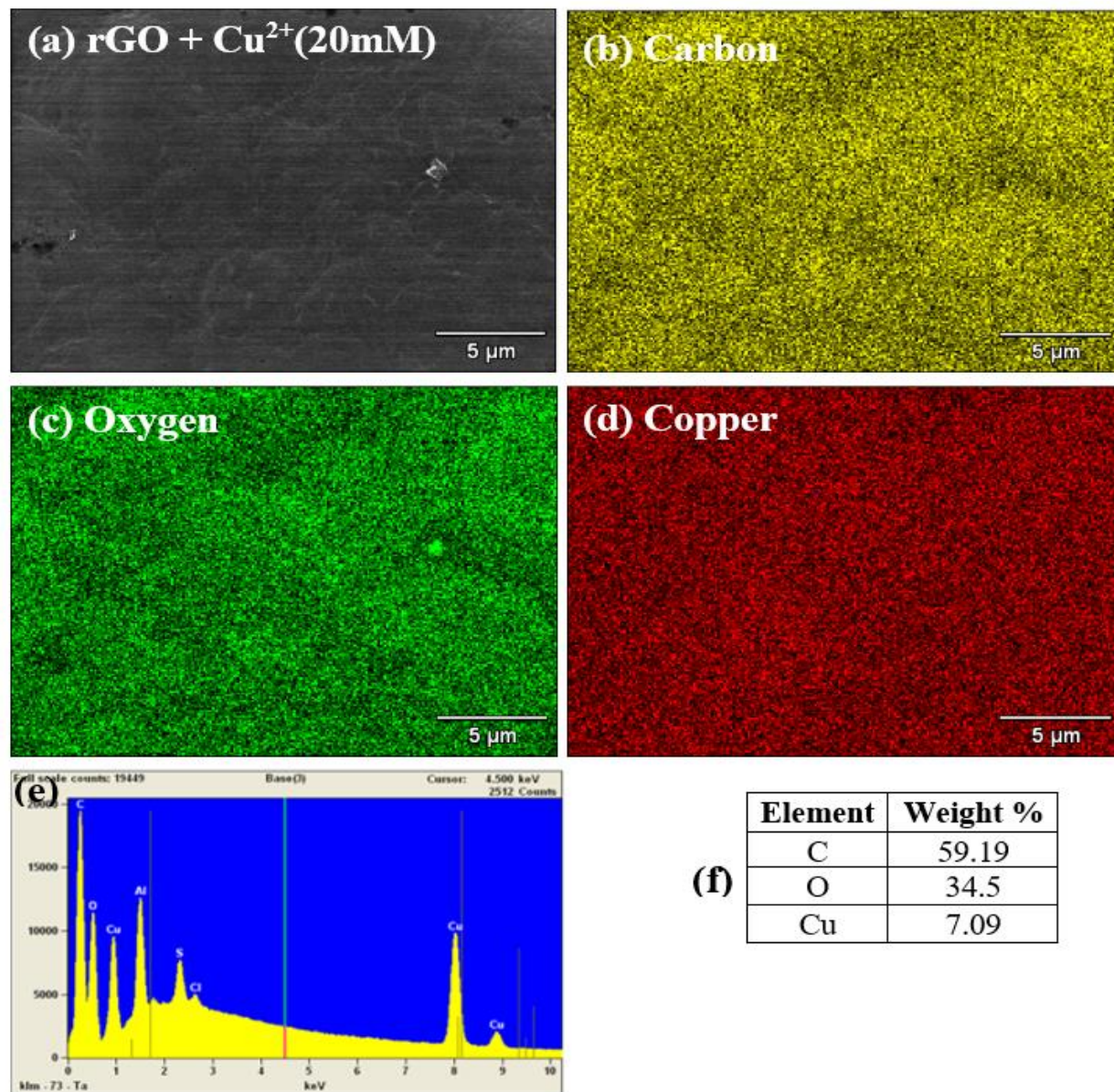


Figure 4.8 (a) SEM image of reduced GO + Cu²⁺ film (50 μ m) with 20 mM CuSO₄ via low temperature thermal reduction (b) Distribution map of carbon over the scanned area of rGO + Cu²⁺ (20 mM) film. (c) Distribution map of oxygen over the scanned area of rGO + Cu²⁺ (20 mM) film (d) Distribution map of copper over the scanned area of rGO + Cu²⁺ (20 mM) film (e) EDS spectrum of rGO film (50 μ m) reduced via thermal reduction (f) Elemental composition of rGO + Cu²⁺ (20 mM) film.

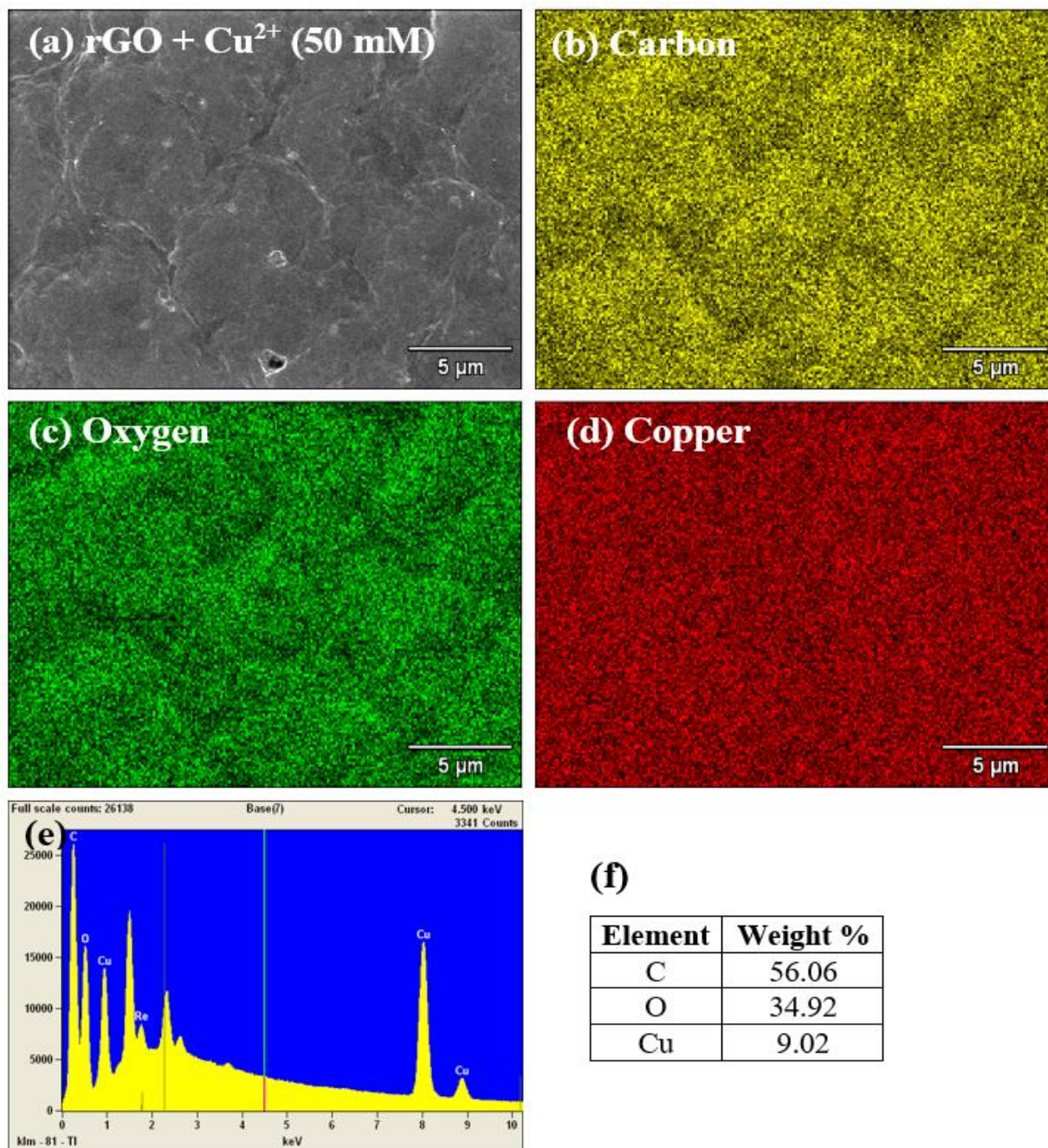


Figure 4.9 (a) SEM image of reduced GO + Cu²⁺ film (50 μm) with 50 mM CuSO₄ via low temperature thermal reduction (b) Distribution map of carbon over the scanned area of rGO + Cu²⁺ (50 mM) film. (c) Distribution map of oxygen over the scanned area of rGO + Cu²⁺ (50 mM) film (d) Distribution map of copper over the scanned area of rGO + Cu²⁺ (50 mM) film (e) EDS spectrum of rGO film (50 μm) reduced via thermal reduction (f) Elemental composition of rGO + Cu²⁺ (50 mM) film.

4.3 FT-IR Spectrum Analysis

4.3.1 FT-IR spectrum of GO and GO + Cu²⁺ thin films

In FT-IR studies for GO (50 μm thin film), absorption peaks appearing at 1726 cm^{-1} , 1620 cm^{-1} , 1598 cm^{-1} are due to C=O, O-H and C=C (aromatic) respectively (Figure 4.10). Furthermore, bands at 1365 cm^{-1} , 1250 cm^{-1} , and 1095 cm^{-1} are due to O-H vibration, epoxy rings and C-O/C-C bending. Similarly, FT-IR studies on GO + Cu²⁺ (with 50 mM Cu²⁺ concentration) were also performed. Figure 4.10 shows the FT-IR spectra of GO and GO + Cu²⁺ (with 50 mM Cu²⁺) free standing thin films of thicknesses 50 μm .

In contrast to the FT-IR spectrum of GO, the relative intensity of C=O in the Cu-containing films decreased and there was a slight shift in the O-H peak in GO + Cu²⁺ thin film. These changes can be attributed to the carboxylic acid coordination with divalent metal ions. This can be also related to cross-linking of GO sheets with divalent metal ions (Cu²⁺). A change in intensity (disappearance of the shoulder) was observed at wavenumber 1365 cm^{-1} , due to the coagulation of Cu²⁺ ions in GO. This change in intensity can be attributed to the epoxy ring opening upon Cu²⁺ addition. Experimental results by Park et al. [31] for increasing the mechanical property of graphene oxide papers with divalent ions (Mg²⁺ and Ca²⁺) showed a similar FT-IR trend.

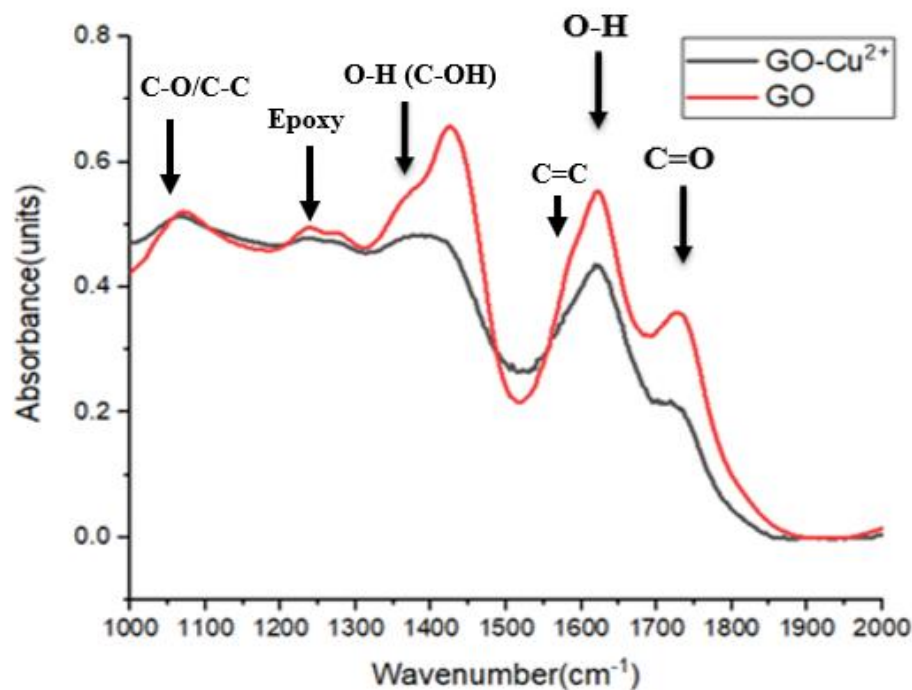


Figure 4.10 Representative FT-IR spectra of GO (50 μm thin film) and GO + Cu^{2+} (with 50 mM Cu^{2+} concentration and 50 μm thin film thickness).

Figure 4.11 shows the FT-IR absorption spectra for GO + Cu^{2+} coagulated with different concentrations of copper ions (Cu^{2+}) in GO; 10, and 50 mM in GO. The addition of Cu appears to result in a decrease in peak intensities at 1400 cm^{-1} (-OH) corresponding to -C-OH, 1250 cm^{-1} (epoxy) and 1726 cm^{-1} (C=O). This change can be related to binding between the Cu^{2+} and the functional groups present in the GO especially -OH (-C-OH) and epoxy ring. Further assessment of the effects of Cu addition will require more detailed analysis, e.g. via curve fitting.

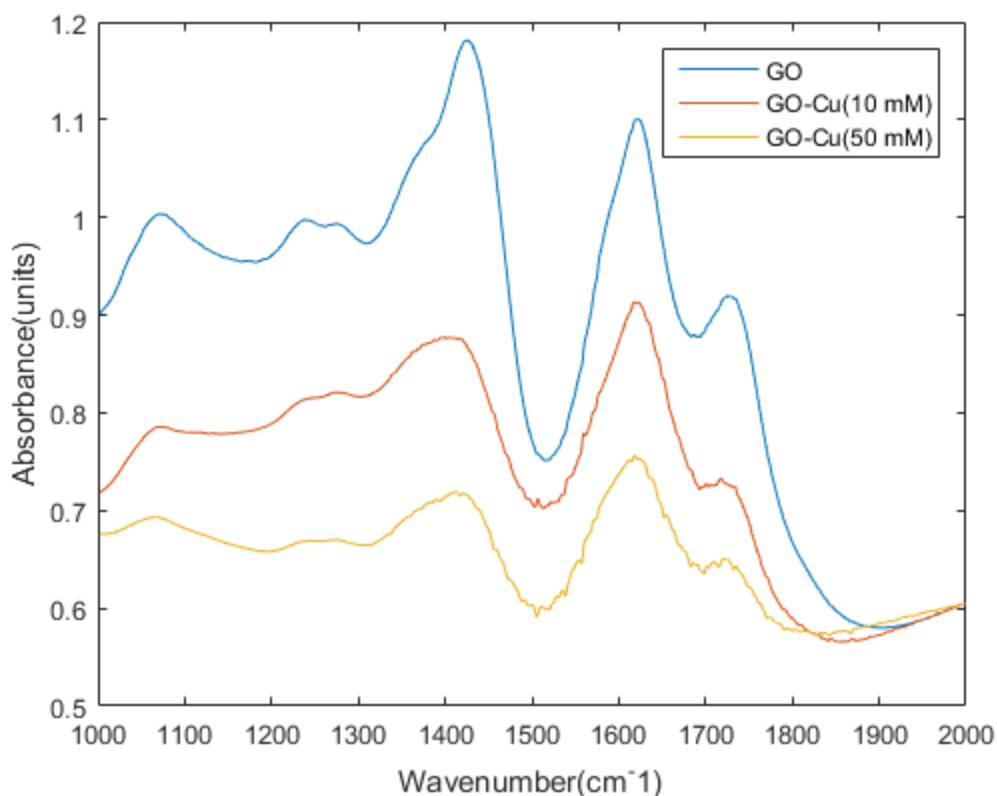


Figure 4.11 Representative FT-IR spectra of GO and GO + Cu²⁺ coagulated with different Cu²⁺ concentrations; 10, and 50 mM.

4.3.2 FT-IR spectrum of thermally reduced rGO + Cu²⁺ thin films with different concentrations of Cu²⁺

The FT-IR spectra of the thermally reduced and laser reduced rGO + Cu²⁺ (50 mM of Cu²⁺) were examined with reference to the FT-IR spectrum of GO + Cu²⁺ (50 mM of Cu²⁺). First, Figure 4.12 shows the FT-IR spectra of GO + Cu²⁺ (with 50 mM Cu²⁺) and thermally reduced rGO + Cu²⁺ (with 50 mM Cu²⁺). The spectra (blue curve) corresponding to thermally reduced rGO + Cu²⁺ (with 50 mM) exhibits an

increase in the C=C (aromatic) vibration at 1592 cm^{-1} (sp^2 restoration) and the epoxy ring vibration at 1250 cm^{-1} . Meanwhile, a decrease in O-H (H_2O) at 1620 cm^{-1} was observed supporting the removal of intercalated water molecules. A decrease in the C=O, C-O vibrations and O-H (C-OH) deformation was also observed, again supporting the removal of oxygen-containing functional groups.

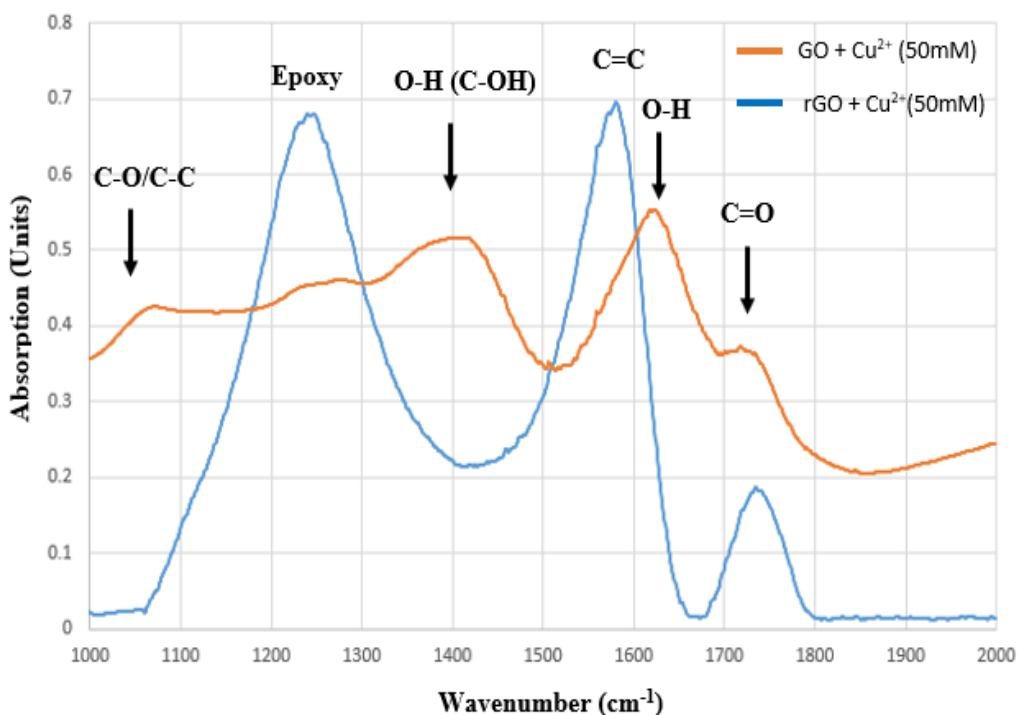


Figure 4.12 Representative FT-IR spectra of GO + Cu^{2+} (50 mM Cu^{2+}) and thermally reduced rGO + Cu^{2+} (50 mM Cu^{2+}).

Figure 4.13 shows the FT-IR spectra of thermally reduced rGO + Cu^{2+} thin films with different concentrations of Cu^{2+} ; 10, 20, and 50 mM. From the figure, it was inferred that after thermal reduction of the GO + Cu^{2+} thin films, C=C (at 1598 cm^{-1}) peak was restored which indicates the restoration of sp^2 hybridization in the thin film. This restoration makes the thin film more conductive which was quantitatively

measured using four-point probe (discussed in the next section). With the increasing C=C vibration with thermal reduction, there was also an accompanying retention and apparent increase in vibrational band intensities associated with epoxy (1250 cm^{-1}) and C=O (1726 cm^{-1}) functional groups. While there does not appear to be a clear trend in vibrational mode intensities with Cu content in the films, the presence of Cu^{2+} may play a role in stabilizing these two functional groups even under the thermal reduction conditions used.

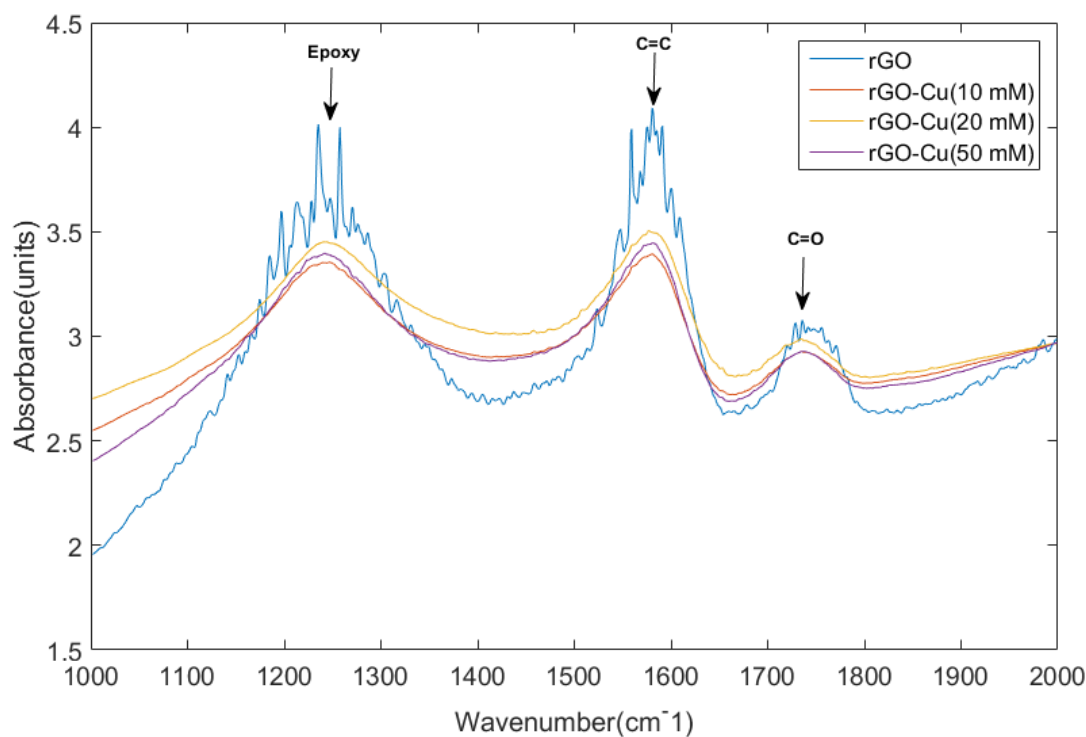


Figure 4.13. Representative FT-IR spectrum of thermally reduced rGO and rGO + Cu^{2+} thin films with different concentrations of Cu^{2+} ; 10, 20, and 50 mM.

4.3.3 FT-IR spectrum of laser reduced GO + Cu²⁺ (50 mM) irradiated with constant power and varying time

In this section, the FT-IR spectra of laser reduced rGO + Cu²⁺ (50 mM Cu²⁺) with a constant power of 0.5 mW/cm² and by varying the exposure time were investigated with reference to unreduced GO + Cu²⁺ (50 mM Cu²⁺). As described earlier, the associated fluence values for combination of laser intensity and times used were 150, 300, 600, 1200, 2400, and 4800 mJ/cm².

Figure 4.14 shows the FT-IR spectra of GO + Cu²⁺ (with 50 mM Cu²⁺) and laser reduced rGO + Cu²⁺ (with 50 mM Cu²⁺) thin films with constant laser power and varying time. With the increase in the laser fluence value, there was large initial decrease observed in the overall intensities of the absorption peaks (epoxy rings at 1250 cm⁻¹, C-C/C-O at 1100 cm⁻¹) associated with the laser reduced rGO + Cu²⁺ (with 50 mM Cu²⁺). The 1598 cm⁻¹ peak, attributed to the reformation of sp² hybridized bonding in the structure (C=C, aromatic) appears to be present adding to the higher energy side of the 1620 cm⁻¹ band and broadening the spectral peak envelope in this range. The overall decrease in absorbance observed for all fluence levels coupled with a lack of significant increase in the aromatic band at 1598 cm⁻¹

indicates that the laser power/fluence conditions were sufficient to cause degradation and likely ablation of the film rather than the targeted reduction behavior.

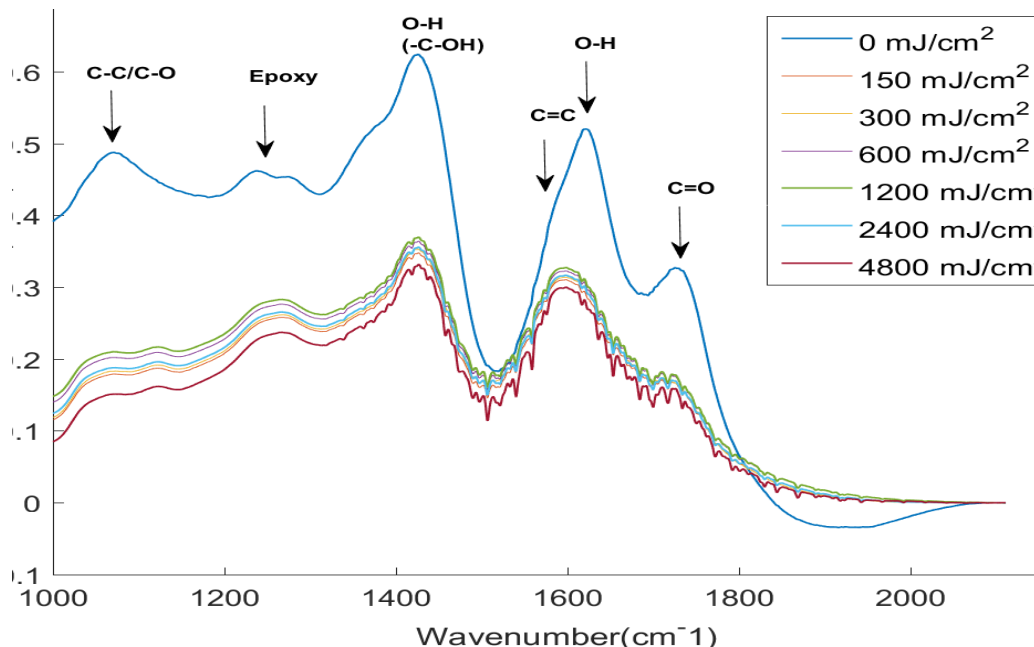


Figure 4.14 Representative FT-IR spectra of laser reduced GO + Cu²⁺(with 50 mM Cu²⁺) at constant power of 0.5 mW/cm² and varying time from 0, 10, 20, 40, 80 and 160 minutes.

4.3.4 FT-IR spectra of laser reduced GO + Cu²⁺ (50 mM) irradiated with constant time and varying power

The FT-IR spectrum of laser reduced GO + Cu²⁺ (50 mM) thin films with constant time and varying power were also examined. The 1×1 cm² thin films were exposed iteratively for an elapsed time period of 5 minutes at increasing beam powers (i.e. 0.08, 0.25, 0.42, and 0.5 mW/cm²) the corresponding fluence values

obtained were 25, 75, 125, and 150 mJ/cm^2 . From this Figure 4.15, an overall decrease in absorbance was observed, again indicating fluence levels that were sufficient to cause film degradation rather than reduction.

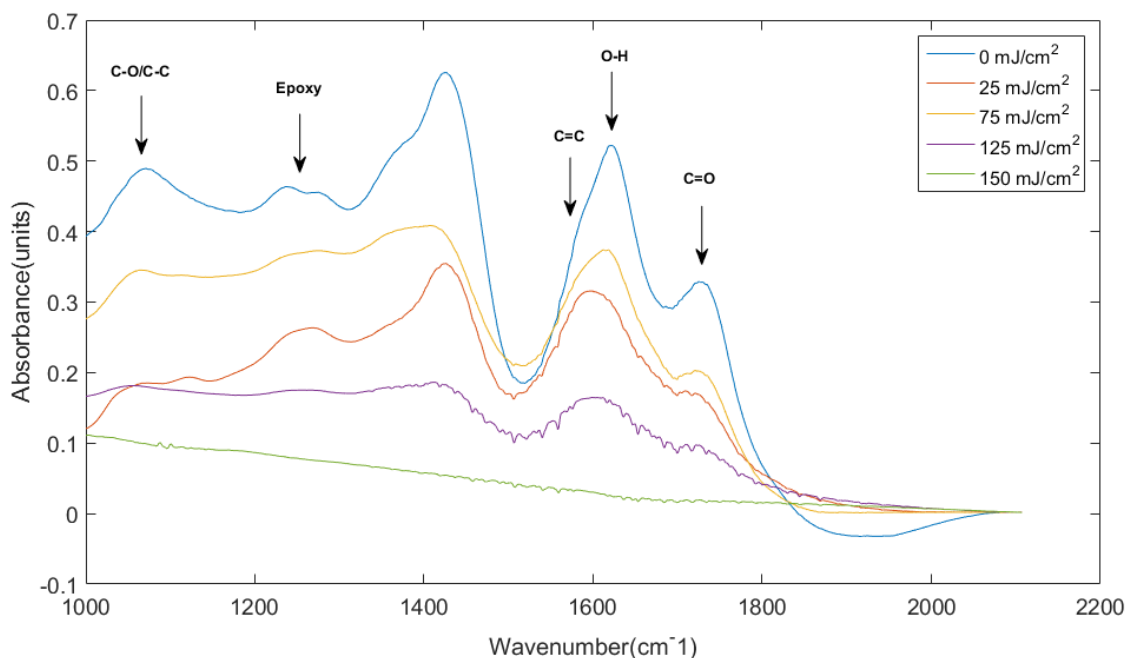


Figure 4.15. FT-IR spectra of laser reduced GO + Cu^{2+} (50 mM Cu^{2+}) thin films for a constant time of 5 minutes and varying power from 0.08, 0.25, 0.42, and 0.5 mW/cm^2 .

Based on these FT-IR spectra it apparent that the photo exposure conditions used produced material degradation rather than reduction (restoration of sp^2 framework). While laser reduction with similar fluence values have been demonstrated in past work, these utilized a pulsed laser source [89] thus illustrating the importance of a full assessment of optical irradiation conditions (rather than just accumulated fluence) on material response. In the present study, the damage occurring is likely related to the continuous wave laser source used in the experiment. In contrast to the

limited duty cycle characteristic of a pulsed source, the continuous energy flux delivered by the CW laser, coupled with the finite energy (heat) dissipation capacity of the specimen and holder arrangement, resulting in much higher temperatures at the specimen surface. These conditions likely led to the material damage behavior observed. With the same fluence values, a pulsed laser with as appropriate repetition rate would have served the reduction process better as there is some time left between each laser pulse for the dissipation of heat from the sample.

4.4 Resistivity measurement using four-point probe

Sheet resistance measurements were performed at ambient conditions with a Bridgetec four-point probe station. An ITO thin film on glass (sheet resistance $\sim 9.1 \text{ k}\Omega/\square$) served as a calibration standard for the system and was measured each time before measuring the sheet resistance of the sample (reduced GO and $\text{GO} + \text{Cu}^{2+}$).

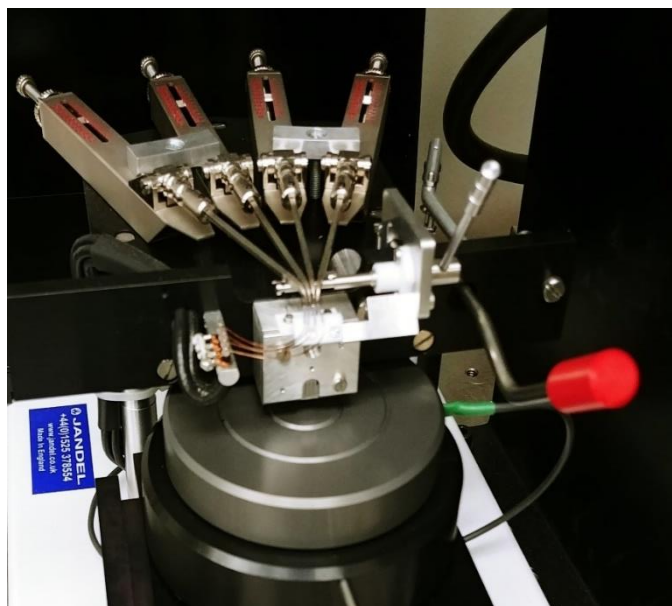


Figure 4.16 Picture of Bridgetec four-point probe.

Figure 4.16 shows the image of the four-point probe with the sample holder on a XY-axis.

The thermal reduction technique was used to reduce the GO and GO + Cu²⁺ films in order to remove the oxygen-containing functional groups and thereby decrease the resistance. Before reduction, the film resistance was too high to allow measurement (contact limit error). To gain insight into carrier transport within the thermally reduced GO and GO + Cu²⁺ free standing thin films, sheet resistance under ambient conditions was evaluated as a function of concentration of Cu²⁺ ions in the film. Figure 4.13 shows the sheet resistance as a function of concentration of Cu²⁺ ions in rGO + Cu²⁺ thermally reduced thin films of thickness 50 μm.

From the Figure 4.17, it is evident that the sheet resistance decreases with increase in the Cu²⁺ concentration in the thermally reduced rGO + Cu²⁺ thin films. The rGO film had a resistivity of 123 KΩ.cm whereas the reduced GO film with 50 mM Cu²⁺ had a resistivity of 20.0 KΩ.cm. There was an increase in the conductivity of the film with increase in the Cu²⁺ concentration in the film. This can be attributed to the cross-linking of divalent Cu²⁺ ions in the layered structure of GO which in turn helps in decreasing the sheet resistance upon thermal reduction. In contrast, the resistivity measurements of all laser reduced materials showed very high values (~MΩ) (contact limit) supporting the earlier interpretation that there had been

significant material degradation rather than reduction of the rGO + Cu²⁺ thin films under the optical exposure conditions used. The damage disrupted the sp² (C-C) network needed for the charge transport.

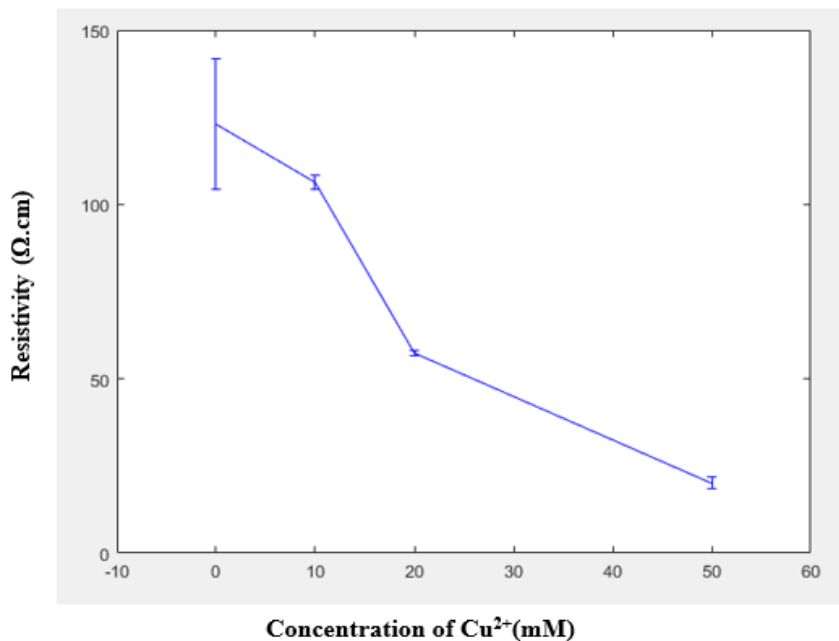


Figure 4.17. Plot showing resistivity of thermally reduced rGO + Cu²⁺ with increase in Cu²⁺ concentration (10, 20, and 50 mM)(kΩ/□) as a function of concentration of Cu²⁺ (mM).

4.5 Conclusion & Future Scope

Solution-processable metal ion (Cu²⁺) coagulated based graphene oxide (GO)/reduced graphene oxide (rGO) nanocomposites are material of interest with potential in various technological applications. In this work, freestanding thin films (μm) were fabricated via doctor blading technique from copper (Cu²⁺) coagulated

graphene oxide dispersion followed by reduction of these films by thermal annealing and laser assisted reduction. Electrical and optical properties of these nanocomposite thin films are characterized using techniques like four-point probe (FPP), Fourier Transform-Infrared spectroscopy (FTIR). An insight into the chemical bonding of the elements in the nanocomposite thin film was provided using X-ray photoelectron spectroscopy and surface morphology changes of the thin films using scanning electron microscopy/electron dispersive spectroscopy (SEM/EDS) before and after the reduction process. It was found that the GO coagulated with Cu^{2+} (thin film with 50 mM Cu^{2+} with 50 μm thickness) dramatically decreases the resistivity upon thermal reduction.

Upon photo exposure of GO + Cu^{2+} (with 50 mM Cu^{2+}) thin films, there was no change observed in the resistivity of the reduced films. In fact, vibrational spectra and resistivity measurements confirm that, under the exposure conditions used, the material was severely degraded rather than reduced, leading to disruption in the sp^2 -hybridization network, which is essential for charge transport. Further assessment of appropriate exposure conditions to produce photo reduction in GO-Cu is required.

Coagulation of divalent-metal ions (Cu^{2+}) in GO dispersion and reduction (thermal and laser reduction) of the GO + Cu^{2+} thin films is discussed in the thesis. However, complete reduction is still difficult to achieve due to the limited understanding of the chemistry and structure of GO, rGO and their coagulated forms.

Therefore, future research should be focused on controllable functionalization of GO, controllable coagulation of GO dispersions and a further investigation of the reduction mechanism for specific applications. Research on oxidation and reduction combined with increased understanding of the graphene structure may enable the realization of improved control over the attachment and elimination of functional groups and multivalent-cations at specific locations on the basal plane of carbon. A well- designed reduction method is needed to remove most of the oxygen functional groups and recover the defective regions. This would, in turn facilitate the applications of graphene as semi-conductors used in electronic and optoelectronic devices.

References

- [1] Geim, A.K. and Novoselov, K.S., "The rise of graphene," *Nature Materials*, pp. 183-191, 2007.
- [2] Novoselov, K.S., et al, "Electric field effect in atomically thin carbon films," *Science*, pp. 666-669, 2004.
- [3] Geim, A.K., "Graphene: Status and Prospects," *Science*, pp. 1530-1534., 2009.
- [4] Zhu, Y.W., Murali, S., Cai, W.W., Li, X.S., Suk, J.W., Potts, J.R., and Ruoff, R.S., "Graphene and Graphene Oxide: Synthesis, Properties, and Applications," *Advanced Materials*, pp. 3906-3924, 2010.
- [5] Weiss, N.O., Zhou, H.L., Liao, L., Liu, Y., Jiang, S., Huang, Y., and Duan, X.F., "Graphene: An Emerging Electronic Material," *Advanced Materials*, pp. 5782-5825, 2012.
- [6] Chua, C.K. and Pumera, M., "Chemical reduction of graphene oxide: a synthetic chemistry viewpoint," *Chemical Society Reviews*, pp. 291-312, 2014.
- [7] Brodie, B.C., "On the Atomic Weight of Graphite," *Philosophical Transactions of the Royal Society of London*, pp. 249-259, 1859.
- [8] L. Staudenmaier, "Verfahren zur Darstellung der Graphitsäure," *Berichte der deutschen chemischen Gesellschaft*, pp. p. 1481-1487., 1898.

- [9] Hofmann, U. and Holst, R., “Über die Säurenatur und die Methylierung von Graphitoxyd,” *Berichte der deutschen chemischen Gesellschaft (A and B Series)*, pp. 754-771, 1939.
- [10] Kovtyukhova, N.I., Ollivier, P.J., Martin, B.R., Mallouk, T.E., Chizhik, S.A., Buzaneva, E.V., and Gorchinskiy, A.D, “Layer-by-layer assembly of ultrathin composite films from micron-sized graphite oxide sheets and polycations,” *Chemistry of Materials*, pp. p. 771-778., 1999.
- [11] Marcano, D.C., Kosynkin, D.V., Berlin, J.M., Sinitskii, A., Sun, Z.Z., Slesarev, A., Alemany, L.B., Lu, W., and Tour, J.M., “Improved Synthesis of Graphene Oxide,” *ACS Nano*, pp. p. 4806-4814, 2010.
- [12] Peng, L., Xu, Z., Liu, Z., Wei, Y., Sun, H., Li, Z., Zhao, X., and Gao, C., “An iron-based green approach to 1-h production of single-layer graphene oxide,” *Nature Communications*, p. p. 5716, 2015.
- [13] Hummers WS, and Offeman RE, “Preparation of graphitic oxide,” *Journal of American Chemical Society*, p. 1339, 1958.
- [14] Zhang, S., Zhu, L.X., Song, H.H., Chen, X.H., Wu, B., Zhou, J.S., and Wang, F., “How graphene is exfoliated from graphitic materials: synergistic effect of oxidation and intercalation processes in open, semi-closed, and closed carbon systems,” *Journal of Materials Chemistry*, pp. 22150-22154, 2012.
- [15] Dimiev, A.M. and Tour, J.M., “Mechanism of graphene oxide formation,” *ACS Nano*, pp. 3060-3068, 2014.
- [16] K.P. Loh, Q. Bao, G. Eda, and M. Chhowalla, “Graphene oxide as Chemically Tunable platform for optical applications,” *Nature Chemistry* 2, p. 1015-1024, 2010.

- [17] Dreyer, D.R., Park, S., Bielawski, C.W., and Ruoff, R.S., "The chemistry of graphene oxide," *Chemical Society Reviews*, pp. 228-240, 2010.
- [18] Dreyer, D.R., Todd, A.D., and Bielawski, C.W., "Harnessing the chemistry of graphene oxide," *Chemical Society Reviews*, pp. 5288-5301, 2014.
- [19] Szabo, T., Berkesi, O., Forgo, P., Josepovits, K., Sanakis, Y., Petridis, D., and Dekany, I., "Evolution of surface functional groups in a series of progressively oxidized graphite oxides," *Chemistry of Materials*, pp. 2740-2749, 2006.
- [20] G. Ruess, "Über das Graphitoxyhydroxyd (Graphitoxyd)," *Monatshefte für Chemie und verwandte Teile anderer Wissenschaften*, pp. 381-417, 1947.
- [21] Scholz, W. and Boehm, H.P., "Untersuchungen am Graphitoxid. VI. Betrachtungen zur Struktur des Graphitoxids," *Zeitschrift für anorganische und allgemeine Chemie*, pp. 327-340, 1969.
- [22] Nakajima, T., Mabuchi, A., and Hagiwara, R., "A New Structure Model of Graphite Oxide," *Carbon*, pp. 357-361, 1988.
- [23] Lerf, A., He, H.Y., Forster, M., and Klinowski, J., "Structure of graphite oxide revisited," *Journal of Physical Chemistry B*, pp. 4477-4482, 1998.
- [24] Erickson, K., Erni, R., Lee, Z., Alem, N., Gannett, W., and Zettl, A., "Determination of the Local Chemical Structure of Graphene Oxide and Reduced Graphene Oxide," *Advanced Materials*, pp. 4467-4472, 2010.
- [25] Rourke, J.P., Pandey, P.A., Moore, J.J., Bates, M., Kinloch, I.A., Young, R.J., and Wilson, N.R., "The Real Graphene Oxide Revealed: Stripping the Oxidative Debris from the Graphene-like Sheets," *Angewandte Chemie-International Edition*, pp. 3173-3177, 2011.

- [26] Thomas, H.R., Valles, C., Young, R.J., Kinloch, I.A., Wilson, N.R., and Rourke, J.P., "Identifying the fluorescence of graphene oxide," *Journal of Materials Chemistry C*, pp. 338-342, 2013.
- [27] S. Stankovich, D. A. Dikin, and G. H. B. Dommett, "Graphene-based composite materials," *Nature*, pp. 282–286, 2006.
- [28] E. Bekyarova, M. E. Itkis, P. Ramesh, C. Berger, and M. Sprinkle, "Chemical Modification of Epitaxial Graphene: Spontaneous Grafting of Aryl Groups," *Journal of the American chemical society*, p. 1336–1337, 2009.
- [29] J. Choi, H. Lee, K.-j. Kim, B. Kim, and S. Kim, "Chemical Doping of Epitaxial Graphene by Organic Free Radicals," *The journal of physical chemistry letters*, p. 505–509, 2010.
- [30] J. Kim, et al., "Graphene Oxide Sheets at Interfaces," *Journal of the American chemical society*, p. 8180–8186, 2010.
- [31] S. Park, K.-S. Lee, G. Bozoklu, W. Cai, S. T. Nguyen and R.S. Ruoff, "Graphene Oxide Papers Modified by Divalent Ions - Enhancing Mechanical Properties via Chemical Cross-Linking," *ACS Nano*, p. 572–578, 2008.
- [32] K.C. Mei, et al., "Organic Solvent-Free, One-Step Engineering of Graphene-Based Magnetic-Responsive Hybrids Using Design of Experiment-Driven Mechanochemistry," *New Carbon Mater*, p. 147–152, 2009.
- [33] Y. Xue, et al, "Oxidizing metal ions with graphene oxide: the in situ formation of magnetic nanoparticles on self-reduced graphene sheets for multifunctional applications," *Chemical Communications*, p. 11689–11691, 2011.
- [34] Wang X., and C. Xu, "Fabrication of flexible metal-nanoparticle films using graphene oxide sheets as substrates," *Small*, p. 2212–2217, 2009.

- [35] H. G. Sudibya, Q. He, H. Zhang and P. Chen, "Electrical Detection of Metal Ions Using Field-Effect Transistors Based on Micropatterned Reduced Graphene Oxide Films," *ACS Nano*, p. 1990–1994, 2011.
- [36] M. Mathesh, J. Liu, N. D. Nam, S. K. H. Lam, R. Zheng, C. J. Barrow and W. Yang, "Facile synthesis of graphene oxide hybrids bridged by copper ions for increased conductivity," *Journal of materials chemistry C*, p. 3084–3090, 2013.
- [37] Kuila, T., Mishra, A.K., Khanra, P., Kim, N.H., and Lee, J.H., "Recent advances in the efficient reduction of graphene oxide and its application as energy storage electrode materials," *Nanoscale*, pp. p. 52-71, 2013.
- [38] Pei, S., and H.-M. Cheng, "The reduction of graphene oxide," *Carbon*, pp. 3210-3228, 2012.
- [39] McAllister, M.J., et al., "Single sheet functionalized graphene by oxidation and thermal expansion of graphite," *Chemistry of Materials*, pp. 4396-4404., 2007.
- [40] Kudin, K.N., Ozbas, B., Schniepp, H.C., Prud'homme, R.K., Aksay, I.A., and Car, R., "Raman spectra of graphite oxide and functionalized graphene sheets," *Nano Letters*, pp. 36-41, 2008.
- [41] Allen, M.J., Tung, V.C., and Kaner, R.B., "Honeycomb Carbon: A Review of Graphene," *Chemical Reviews*, pp. 132-145, 2010.
- [42] Wang, X., Zhi, L.J., and Mullen, K., "Transparent, conductive graphene electrodes for dye-sensitized solar cells," *Nano Letters*, pp. 323-327, 2008.
- [43] Valles, C., Nunez, J.D., Benito, A.M., and Maser, W.K., "Flexible conductive graphene paper obtained by direct and gentle annealing of graphene oxide paper," *Carbon*, pp. 835-844, 2012.
- [44] A. Oberlin, "Carbonization and Graphitization," *Carbon*, pp. 521-541, 1984.

- [45] S. Liu, et al., “Low temperature in-situ preparation of reduced graphene oxide/ZnO nanocomposites for highly sensitive photodetectors,” *Journal of Materials Science Materials in Electronics*, vol. 28, no. 13, pp. 9403-9409, 2017.
- [46] Eigler, S. and Hirsch, A., “Chemistry with Graphene and Graphene Oxide—Challenges for Synthetic Chemists,” *Angewandte Chemie International Edition*, vol. 53, no. 30, pp. 7720-7738, 2014.
- [47] Bai H, Li C, and Shi G., “Functional composite materials based on Chemically converted Graphene,” *Advanced Materials*, vol. 23, no. 9, p. 1089–1115, 2011.
- [48] P. Sungjin, et al., “Hydrazine-reduction of graphite- and graphene oxide,” *Carbon*, vol. 49, no. 9, p. 3019 – 3023, 2011.
- [49] Li, D., Muller, M.B., Gilje, S., Kaner, R.B., and Wallace, G.G, “Processable aqueous dispersions of graphene nanosheets,” *Nature Nanotechnology*, pp. 101-105, 2008.
- [50] Pei, S.F., Zhao, J.P., Du, J.H., Ren, W.C., and Cheng, H.M., “Direct reduction of graphene oxide films into highly conductive and flexible graphene films by hydrohalic acids,” *Carbon*, vol. 48, no. 15, pp. 4466-4474, 2010.
- [51] Moon, I.K., Lee, J., Ruoff, R.S., and Lee, H., “Reduced graphene oxide by chemical graphitization,” *Nature Communications*, vol. 73, 2010.
- [52] Fernandez-Merino, M.J., “Vitamin C Is an Ideal Substitute for Hydrazine in the Reduction of Graphene Oxide Suspensions,” *Journal of Physical Chemistry C*, vol. 114, no. 14, pp. 6426-6432, 2010.
- [53] Zhang, J.L., Yang, H.J., Shen, G.X., Cheng, P., Zhang, J.Y., and Guo, S.W, “Reduction of graphene oxide via L-ascorbic acid,” *Chemical Communications*, vol. 46, no. 7, pp. 1112-1114, 2010.

- [54] Dreyer, D.R., Murali, S., Zhu, Y.W., Ruoff, R.S., and Bielawski, C.W, "Reduction of graphite oxide using alcohols," *Journal of Materials Chemistry*, vol. 21, no. 10, pp. 3443-3447, 2011.
- [55] Zhu, C.Z., Guo, S.J., Fang, Y.X., and Dong, S.J., "Reducing Sugar: New Functional Molecules for the Green Synthesis of Graphene Nanosheets," *ACS Nano*, vol. 4, no. 4, pp. 2429-2437, 2010.
- [56] Kuila, T., Mishra, A.K., Khanra, P., Kim, N.H., and Lee, J.H., "Recent advances in the efficient reduction of graphene oxide and its application as energy storage electrode materials," *Nanoscale*, vol. 5, no. 1, pp. 52-71, 2013.
- [57] Zhu, Y.W., Murali, S., Stoller, M.D., Velamakanni, A., Piner, R.D., and Ruoff, R.S., "Microwave assisted exfoliation and reduction of graphite oxide for ultracapacitors," *Carbon*, vol. 48, no. 7, pp. 2118-2122, 2010.
- [58] G. Williams, B. Seger, and P.V. Kamat, "TiO₂-Graphene Nanocomposites: UV-assisted photocatalytic reduction of graphene oxide," *ACS Nano*, vol. 2, no. 7, pp. 1487-1491, 2008.
- [59] O. Akhavan, and E. Ghaderi, "Photocatalytic reduction of graphene oxide nanosheets on TiO₂ thin film for photoinactivation of bacteria in solar light irradiation," *Journal of physical chemistry C*, vol. 113, no. 47, pp. 20214-20220, 2009.
- [60] Y. Zhou, et al., "Microstructuring of graphene oxide nanosheets using direct laser writing," *Advanced Materials*, vol. 22, no. 1, pp. 67-71, 2009.
- [61] L.J. Cote, R.C. Silva, and J.X. Huang, "Flash reduction and patterning of graphite oxide and its polymer composite," *Journal of the American Chemical Society*, vol. 131, no. 31, pp. 11027-11032, 2009.

- [62] V. Abdelsayed, S. Moussa, H.M. Hassan, H.S. Aluri, M.M. Collinson, and M. Samy El-Shall, "Photothermal deoxygenation of graphite oxide with laser excitation in solution and graphene-aided increase in water temperature," *Journal of physical chemistry letters*, vol. 1, no. 19, pp. 2804-2809, 2010.
- [63] L. Huang, Y. Liu, L. -C. Ji, Y. -Q. Xie, T. Wang, and W. -Z. Shi, "Pulsed laser assisted reduction of graphene oxide," *Carbon*, vol. 49, no. 7, pp. 2431-2436, 2011.
- [64] Denis A. Sokolov, Yurii V. Morozov, Matthew P. McDonald, Felix Vietmeyer, Jose H. Hodak, and Masaru Kuno, "Direct Observation of Single Layer Graphene Oxide Reduction through Spatially Resolved, Single Sheet Absorption/Emission Microscopy," *Nano Letters*, vol. 14, no. 6, p. 3172–3179, 2014.
- [65] O. L. Stroyuk, N. S. Andryushina, S. Ya. Kuchmy, and V. D. Pokhodenko, "Photochemical Processes Involving Graphene Oxide," *Theoretical and Experimental Chemistry*, vol. 51, no. 1, pp. 1-29, 2015.
- [66] R. J. W. E. Lahaye, H. K. Jeong, C. Y. Park, and Y. H. Lee, "Density functional theory study of graphite oxide for different oxidation levels," *Physical Review B*, vol. 79, no. 12, 2009.
- [67] S. Wang, et al., "High Mobility, Printable, and Solution-Processed Graphene Electronics," *Nano Letters*, vol. 10, no. 1, pp. 92-98, 2010.
- [68] K. Chen, et al., "Hg(II) Ion Detection Using Thermally Reduced Graphene Oxide Decorated with Functionalized Gold Nanoparticles," *Analytical Chemistry*, vol. 84, no. 9, p. 4057–4062, 2012.
- [69] Q. He, S. Wu, Z. Yina, and H. Zhang, "Graphene-based electronic sensors," *Chemical Science*, vol. 3, no. 6, pp. 1764-1772, 2012.

- [70] H. A. Becerril, J. Mao, Z. Liu, R. M. Stoltenberg, Z. Bao, and Y. Chen, "Evaluation of Solution-Processed Reduced Graphene Oxide Films as Transparent Conductors," *ACS Nano*, vol. 2, no. 3, p. 463–470, 2008.
- [71] P. Matyba, H. Yamaguchi, G. Eda, M. Chhowalla, L. Edman, and N. D. Robinson, "Graphene and Mobile Ions: The Key to All-Plastic, Solution-Processed Light-Emitting Devices," *ACS Nano*, vol. 4, no. 2, p. 637–642, 2010.
- [72] Y. Zhu, et al., "Carbon-Based Supercapacitors Produced by Activation of Graphene," *Science*, vol. 332, no. 6037, pp. 1537-1541, 2011.
- [73] S. Yang, X. Feng, S. Ivanovici, and K. Mullen, "Fabrication of Graphene-Encapsulated Oxide Nanoparticles: Towards High-Performance Anode Materials for Lithium Storage," *Angewandte Chemie*, vol. 49, no. 45, pp. 8408-8411, 2010.
- [74] G. Zhou, et al., "Graphene-Wrapped Fe₃O₄ Anode Material with Improved Reversible Capacity and Cyclic Stability for Lithium Ion Batteries," *Chemistry of Materials*, vol. 22, no. 18, p. 5306–5313, 2010.
- [75] S. C. Ray, "Applications of Graphene and Graphene-Oxide Based Nanomaterials," Elsevier, 2015.
- [76] John Wolstenholme, and J.F. Watts, "An Introduction to Surface Analysis by XPS and AES," John Wiley & Sons, 2005.
- [77] KEIT Spectrometers, "Light path schematic of Michelson FTIR model showing moving mirror arm," 2015. [Online]. Available: <https://keit.co.uk/rugged-ftir-spectroscopy-technology/figure-1/>. [Accessed Saturday May 2018].
- [78] D. Konios, M. M. Stylianakis, E. Stratakis, and E. Kymakis, "Dispersion behaviour of graphene oxide and reduced graphene oxide," *Journal of Colloid and Interface Science*, vol. 430, p. 108–112, 2014.

- [79] G. Patrick, "Project educate," Tuesday October 2014. [Online]. Available: <https://projecteducate.deviantart.com/blog/462654632/>. [Accessed may 2018].
- [80] C. Fu, G. Zhao, H. Zhang, and S. Li, "Evaluation and Characterization of Reduced Graphene Oxide Nanosheets as Anode Materials for Lithium-Ion Batteries," Engineering Research Academy of Graphite New Materials, vol. 8, pp. 6269 - 6280, 2013.
- [81] J. Chan, "Four-point probe manual," Monday April 1994. [Online]. Available: <http://four-point-probes.com/four-point-probe-manual/>. [Accessed Saturday May 2018].
- [82] Novoselov KS, V. I Fal'ko, Colombo L, Gellert PR, Schwab MG, and K.Kim, "A roadmap for graphene," Nature, vol. 490, p. 192–200, 2012.
- [83] Chun Li, and Gaoquan Shi, "Three-dimensional graphene architectures," Nanoscale, vol. 4, no. 18, p. 5549–63, 2012.
- [84] Ji Chen, Bowen Yao, Chun Li, and Gaoquan Shi, "An improved Hummers method for eco-friendly synthesis of graphene oxide," Carbon, vol. 64, p. 225 – 229, 2013.
- [85] Yan Geng, Shu Jun Wang, and Jang Kyo-Kim, "Preparation of graphite nanoplatelets and graphene," Journal of Colloid and Interface Science, vol. 336, no. 2, pp. 592-598, (2009).
- [86] Aegerter, M. A., and Mennig, M., "Sol-Gel Technologies for Glass Producers and Users," New York: Springer, USA, 2004.
- [87] Heyong He, Jacek Klinowski, Michael Forster, and Anton Lerf, "A new structural model for graphite oxide," Chemical Physical Letters, vol. 287, no. 1-2, pp. 53-56, 1998.

- [88] Zhong-li Wang, Dan Xu, Yun Huang, Zhong Wu, Li-min Wang, and Xin-bo Zhang, "Facile, mild and fast thermal-decomposition reduction of graphene oxide in air and its application in high-performance lithium batteries," *Chemical Communications*, vol. 48, no. 7, pp. 976-978, 2012.
- [89] Lei Huang, Yang Liu, Le-Chun Ji, Yi-Qun Xie, Tao Wang, Wang-Zhou Shi, "Pulsed laser assisted reduction of graphene oxide," *Carbon*, vol. 52, pp. 574-582